AD-A148 453 PREDICTION OF DYNAMIC STALL CHARACTERISTICS USING ADVANCED NON-LINEAR PAN..(U) ANALYTICAL METHODS INC REDMOND WA B MASKEW ET AL. 04 APR 84 AMI-8406 1/1

UNCLASSIFIED AFOSR-TR-84-0975 F49620-82-C-0019 F/G 20/4 NL

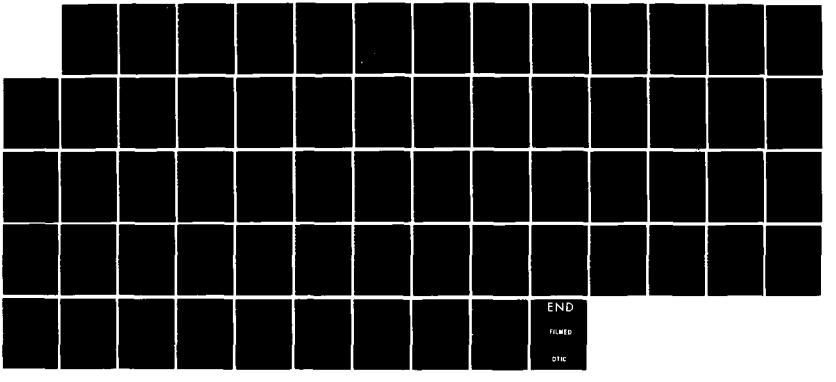

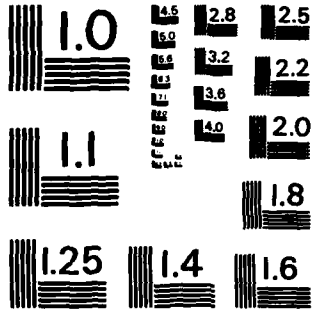

MICROCOPY RESOLUTION TEST CHART
NATIONAL BUREAU OF STANDARDS-1963-A

(12)

Analytical Methods Report 8406

FINAL REPORT

PREDICITON OF DYNAMIC STALL CHARACTERISTICS USING ADVANCED NON-LINEAR PANEL METHODS

B. Maskew and F.A. Dvorak

April 1984

Prepared under Contract F49620-82-C-0019

Submitted to:

AFOSR/NA
Bolling Air Force Base, D.C. 20332

Submitted by:

Analytical Methods, Inc.
2047 - 152nd Avenue N.E.
Redmond, Washington 98052
(206) 643-9090

Qualified requestors may obtain additional copies from the Defense Technical Information Service.

UNCLASSIFIED

SECURITY CLASSIFICATION OF THIS PAGE

REPORT DOCUMENTATION PAGE

1a. REPORT SECURITY CLASSIFICATION UNCLASSIFIED	1b. RESTRICTIVE MARKINGS
2a. SECURITY CLASSIFICATION AUTHORITY	3. DISTRIBUTION/AVAILABILITY OF REPORT Approved for Public Release; Distribution Unlimited.
2b. DECLASSIFICATION/DOWNGRADING SCHEDULE	
4. PERFORMING ORGANIZATION REPORT NUMBER(S) AMI Report 8406	5. MONITORING ORGANIZATION REPORT NUMBER(S) AFOSR-TR- 84-0975
6a. NAME OF PERFORMING ORGANIZATION ANALYTICAL METHODS, INC	6b. OFFICE SYMBOL (If applicable)
6c. ADDRESS (City, State and ZIP Code) 2047 - 152ND AVENUE, NE REDMOND, WA 98052	7a. NAME OF MONITORING ORGANIZATION AFOSR/NA 7b. ADDRESS (City, State and ZIP Code) Bolling AFB, DC.
8a. NAME OF FUNDING/SPONSORING ORGANIZATION AIR FORCE OFFICE OF SCIENTIFIC RESEARCH	8b. OFFICE SYMBOL (If applicable) AFOSR/NA
8c. ADDRESS (City, State and ZIP Code) BOLLING AFB, DC 20332	9. PROCUREMENT INSTRUMENT IDENTIFICATION NUMBER F49620-82-C-0019

10. SOURCE OF FUNDING NOS.			
PROGRAM ELEMENT NO.	PROJECT NO.	TASK NO.	WORK UNIT NO.
61102F	2307	A2	

11. TITLE (Include Security Classification) PREDICTION OF DYNAMIC STALL CHARACTERISTICS USING ADVANCED NON-LINEAR PANEL METHODS (UNCLASSIFIED)

12. PERSONAL AUTHOR(S)
B MASKEW F A DVORAK

13a. TYPE OF REPORT	13b. TIME COVERED	14. DATE OF REPORT (Yr., Mo., Day)	15. PAGE COUNT
FINAL	FROM 1NOV82 TO 17APR84	1984, April 4	56

16. SUPPLEMENTARY NOTATION

17. COSATI CODES		
FIELD	GROUP	SUB. GR.

18. SUBJECT TERMS (Continue on reverse if necessary and identify by block number)
UNSTEADY COUPLED VISCOUS/
TIME-STEPPING CALCULATIONS INVISCID CALCULATION
DYNAMIC SEPARATED WAKE MODEL

19. ABSTRACT (Continue on reverse if necessary and identify by block number)

A surface singularity panel method ~~has been~~ was extended for modeling the dynamic interaction between a separated wake and a surface undergoing an unsteady motion. The method combines the capabilities of an unsteady, time-stepping code and a technique for modeling extensive separation using free vortex sheets. Routines ~~have been~~ were developed for treating the dynamic interaction between the separated wake and the solid boundary in an environment where the separation point is moving with time. The behavior of these routines is being examined in a parallel effort using a two-dimensional pilot version of the three-dimensional code. This allows refinements in the procedures to be quickly developed and tested prior to installation into the main code.

20. DISTRIBUTION/AVAILABILITY OF ABSTRACT	21. ABSTRACT SECURITY CLASSIFICATION
UNCLASSIFIED/UNLIMITED ☒ SAME AS RPT ☐ DTIC USERS ☐	UNCLASSIFIED

22a. NAME OF RESPONSIBLE INDIVIDUAL	22b. TELEPHONE NUMBER (Include Area Code)	22c. OFFICE SYMBOL
MICHAEL S FRANCIS, Major, USAF	202/767-4935	AFOSR/NA

DD FORM 1473, 83 APR EDITION OF 1 JAN 73 IS OBSOLETE

UNCLASSIFIED

SECURITY CLASSIFICATION OF THIS PAGE

The extended code has been coupled with an unsteady integral boundary layer method to examine the prediction of dynamic stall characteristics. The boundary layer code is accessed during the time-step cycle and provides the separation locations as well as the boundary layer displacement effect: the latter is modelled in the potential flow code using the source transpiration technique.

The preliminary results presented here include basic unsteady test cases for both the potential flow and boundary layer routines. Some exploratory separated flow calculations are included from a series of numerical studies on the stability of the calculation procedure. Some preliminary correlations with experimental results are included.

TABLE OF CONTENTS

LIST OF FIGURES

LIST OF FIGURES (CONCLUDED)

1.0 INTRODUCTION

Flow separation on the lifting surfaces of a vehicle at high angle of attack is always complicated by a certain degree of unsteadiness, but, when the vehicle itself is undergoing unsteady motion or deformation, or if it enters a different flow field rapidly, then the complexity of the separated flow is even greater, and culminates in the phenomenon of dynamic stall. If the angle of attack oscillates around the static stall angle, the fluid dynamic forces and moments usually exhibit large amounts of hysteresis and a condition of negative aerodynamic damping often develops during part of the cycle. This can lead to the condition of flutter in a single degree of freedom oscillating rigid body motion. (Normally, in attached flow, flutter only occurs when the body motion includes multiple degrees of freedom; e.g., combined bending and torsion of an aircraft wing.) During a rapid increase in angle of attack, the static stall angle can be greatly exceeded, resulting in excursions in the dynamic force and moment values that are far greater than their static counterparts. The consequences of dynamic stall are far-reaching and lead to such problems as wing drop, yaw (sometimes leading to spin entry), wing rocking and buffeting as well as stall flutter.

Although a great deal has been learned about dynamic stall characteristics--mainly through experimental observation--there is not at this time a completely satisfactory theoretical method (1), (2) for predicting the dynamic stall characteristics for new untested shapes, even for the two-dimensional case. Moreover, quantitative comparisons of experimental test data on new geometries can be obscured by the effects of three-dimensional wind-tunnel interactions, wall interference and experimental uncertainties (3). In the present work a possible theoretical approach is examined for predicting dynamic stall characteristics. The approach combines an unsteady time-stepping method (4) with a steady inviscid/viscid iterative code (5) that includes an extensive separation model. The latter has proven very successful in the steady case. Both codes are applicable to general three-dimensional shapes and have been developed from the same basic panel method (6).

Extensive investigations of the dynamic stall characteristics of airfoils oscillating in pitch have been reviewed by McCroskey (1), (2). In practical aerodynamic environments, the unsteadiness can be a combination of several motions. Unsteady motions other than pitching have been investigated by, among others, Liiva et al. (7), Lang (8), and Francis (9), Maresca et al. (10), and Saxena et al. (11). In these references the phenomena of plunging, flap, spoiler and rectilinear oscillations were examined. There are very few theoretical approaches, however, and in a recent review, McCroskey (2) concludes that at the present time the engineer who needs answers should turn to one of the empirical correlation techniques, even though these are

not completely satisfactory and only supply broad details of force and moment characteristics. The method of Ericson and Reding is perhaps one of the most comprehensive of these methods. Their latest paper (12) incorporates a number of findings from the systematic experiments of Carr et al. (13).

Early theoretical approaches to dynamic stall addressed the deep stall aspect which is dominated by the passage of vortices shed from the vicinity of the leading edge. Ham (14) used just a thin plane model of the airfoil. Later work by Baudu et al. (15) extended the basic model to thick sections using a panel method. The main drawback with the approach is that crucial assumptions regarding the location and time of vortex shedding have to be made in order to perform the calculations. Also, the results (from (15)) are sensitive to (a) the angle at which the vortex path leaves the surface, (b) the time at which vortex emissions terminate so as to start the reattachment process and (c) the viscous diffusion of the free vortices.

Calculations of the characteristics of the thin boundary layer in the attached flow regions of an oscillating airfoil using unsteady methods (16), (17), have demonstrated good qualitative agreement with experimental observations. However, one feature at least needs further examination in regard to improved modeling: it is reported (18), (19) that when incidence is increasing beyond the static stall angle, the location of zero skin friction in the turbulent boundary layer and the catastrophic separation can occur at different stations, Figure 1. Apparently, a long thin tongue of this reversed flow precedes the main separation zone. This is not observed under quasi-steady conditions.

Crimi and Reeves (20) combined a potential flow method with an unsteady boundary layer analysis in a viscous/inviscid interaction approach. The potential flow model was based on chordline singularities and so excluded modeling of the thick wake. Also, detail of the stagnation point location in relation to the curved leading edge was missing. Emphasis was placed on the details of leading-edge bubble bursting and application to trailing-edge separation was not attempted. Shamroth and Kreskovsky (21) developed a similar technique but with improved treatment of the separated flow region, transition phenomena and potential flow region. However, the procedure failed to predict the flow field about the stalled airfoil. They concluded that the effect on the outer inviscid solution due to the finite wake displacement must be modelled.

In spite of the shortcomings of the above approaches, the general technique of matching various viscous and inviscid regions remains an attractive alternative to the full Navier-Stokes treatment. Although, in principle, the latter can overcome limitations of the potential flow/boundary layer iterative approach,

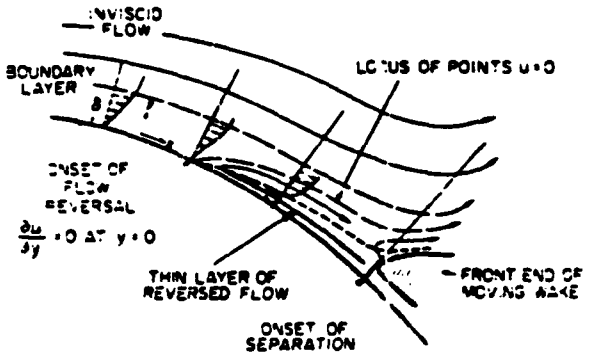

Figure 1. The Model of Sears and Telionis (19) for Upstream-Moving Separation of an Unsteady Boundary Layer.

such treatment is limited at this time to laminar flows at Reynolds numbers much lower than realistic for most practical applications (2). Progress towards higher Reynolds numbers is being made, but applications to general problems is still a long way away (22).

The present method goes beyond the capabilities of the earlier theoretical approaches in that both trailing-edge and leading-edge stall with vortex passage can be included in principle. The method, developed for the three-dimensional case, is applicable to arbitrary configurations and to general motions; i.e., not just pitch oscillation. In addition, because the basis of the method is a surface singularity panel code, a more reliable and direct coupling between the inviscid and viscous analysis is assured. Moreover, modeling of the separated zone in the trailing-edge region and more detailed treatment of the vortex/surface interaction should make the approach more viable for applications to dynamic separation problems.

2.0 POTENTIAL FLOW METHODS

2.1 General

Although remarkable advances are being made in flow field calculations using finite-difference and also finite-element methods, the surface integral approach using panel methods coupled with special routines for nonlinear effects still offers distinct advantages for many real flow problems. In particular, panel methods offer greater versatility for practical application to complicated configurations and are considerably more efficient in terms of computing effort. However, the concept of zonal modeling--in which a local Navier-Stokes analysis is coupled with a panel method--should not be overlooked. Ultimately, such a coupling should lead to an improved modeling of vortices (e.g., vortex cores, vortex dissipation and breakdown), thick viscous regions, local separation bubbles, and shock wave/boundary interactions.

Over the past decade, panel methods have seen a trend toward higher-order formulations (23), (25) and (26). At the outset it was argued that compared with the earlier low-order methods the more continuous representation of the surface singularity distribution should allow a reduction in panel density for a given solution accuracy and, hence, should lead to lower computing costs. No such benefits have appeared so far for the general three-dimensional case. In fact, preliminary investigations (27) have indicated that the prediction accuracy for problems with complicated interactions, such as vortex/surface or high curvature situations, depends more on the density of control points where the boundary conditions are enforced; the order of the singularity distribution plays a minor role. In the meantime, further developments of piecewise constant singularity panel methods, e.g., Morino (28) and AMI's Program VSAERO (6), are giving comparable accuracy to the higher order methods at much lower computing costs.

The low computing cost of Program VSAERO makes it practical to apply the method to nonlinear problems requiring iterative solutions, e.g., wake relaxation for high-lift configurations, multiple-component problems and rotor cases; and viscous/inviscid calculations with coupled boundary layer analyses, including the case with extensive separation (5), and also time-stepping calculations for three-dimensional unsteady problems (4) that are beyond the scope of a harmonic analysis. This method, therefore, offers an attractive basis for a practical tool aimed at predicting the aerodynamic characteristics of dynamic stall problems. At the outset, this code was being developed in two different directions; viz, one was for extensive separation modeling under the "steady" conditions, while the other was for unsteady time-stepping calculations. These two capabilities, described in the section below, have now been brought together in one code.

2.2 Separated Flow Model

Under essentially steady conditions, the pressure distribution in a trailing-edge separation region is usually characterized by a constant pressure region extending back to the trailing edge followed by a short recompression region (e.g., (29)). A simplification of this characteristic is modelled in the two-dimensional CLMAX program (30), (31) using a pair of constant strength vortex sheets to enclose the separated region, Figure 2. The length of the sheets required a semi-empirical approach and the condition that the sheets be force-free is satisfied in an interactive cycle in which segments of the sheet are aligned with calculated local flow directions. The method combines boundary layer and potential flow codes in an outer inviscid/viscid iteration cycle. The potential flow pressure distribution--which includes the influence of the free vortex sheets--is passed to the boundary layer routine which then supplies the separation points and the boundary layer displacement thickness distribution for the next iteration. The boundary layer displacement effect in the attached flow region is modelled by transpiration (i.e., source distribution) rather than by a displacement surface. The main advantage of the transpiration approach is that the matrix of influence coefficients in the panel method remains essentially the same from one iteration to the next; only the wake condition changes.

The thin vortex sheet model of the upper separated shear layer was demonstrated by Young and Hoad (32) to be a reasonable representation of the flow as far back as the trailing edge. For example, a comparison from (32) of a laser-velocimeter flow survey, and CLMAX program calculation is shown here in Figure 3. Downstream of the trailing edge the vortex sheet model becomes less representative of the flow; however, a later evaluation of a graded vorticity model over the recompression zone showed little effect on the airfoil solution. More detailed modeling of the recompression zone (such as, for example, the approaches used by Gross (33) or Zumwalt (34) would be desirable in cases where the wake interacts closely with a downstream component.

A particular feature of the vortex sheet model enclosing the region of low energy is that pressure can be calculated directly in the separated zone (30). This is an additional advantage over the displacement surface approach of Henderson (35) and over the source outflow model of Jacob (36). The CLMAX method generally gives very close agreement with experimental pressure distributions (30), (31). An initial extension of this method to the unsteady case is reported in (31) where quasi-steady solutions coupled with a phase shift model were used. Extension of the model to the three-dimensional case is reported in (37) for a stripwise model and in (5) for a more general treatment. The separation model has also been successfully installed in a transonic finite-difference code (38).

Region 1 - Potential Flow Region
Region 2 - Boundary Layer
Region 3 - Free Shear Layer
Region 4 - Wake

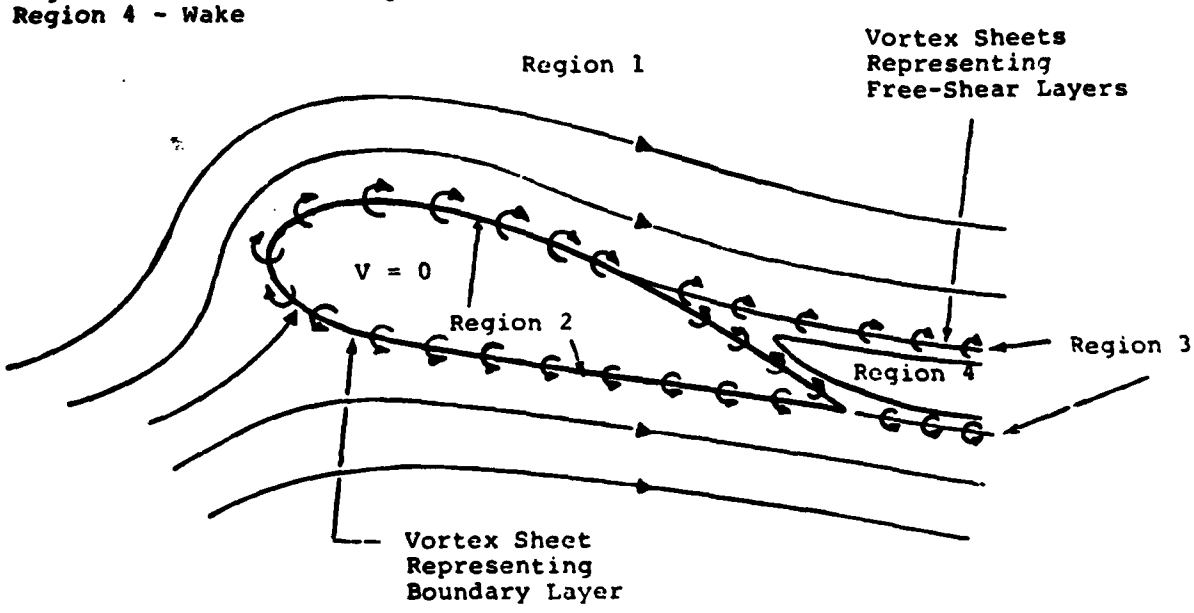

Figure 2. Mathematical Flow Model (Steady).

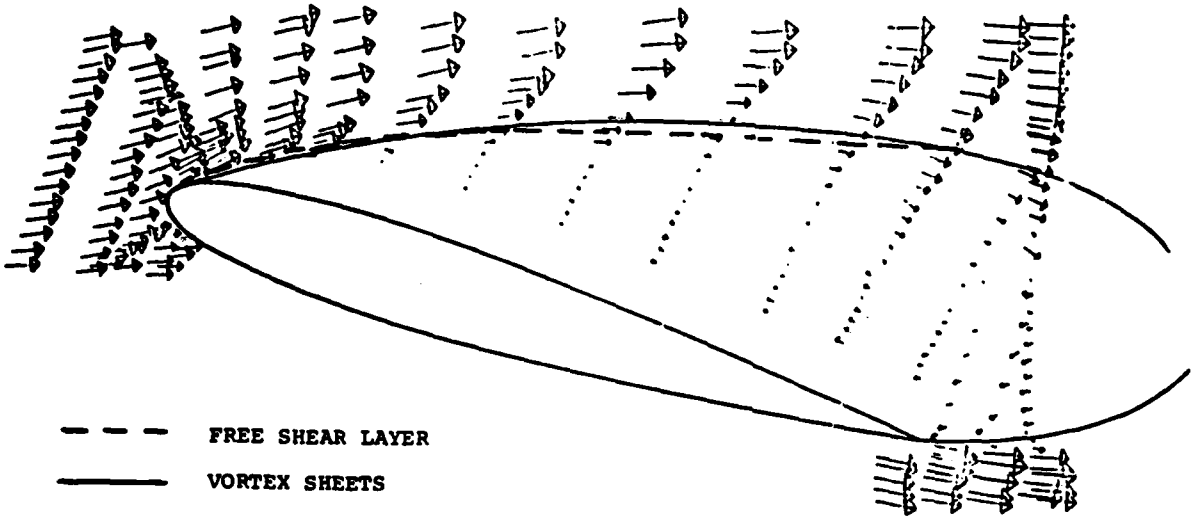

Figure 3. Location of Experimental Free Shear Layer and CLMAX Calculated Vortex Sheet Centerlines for Low Mach Number Case (from (32)).

The same basic model is also applicable for the unsteady case; here, however, the assumption of constant vorticity is no longer valid. In fact, a dynamic wake model is essential and will be discussed below after the description of the unsteady formulation.

2.3 Unsteady Method

2.3.1 Formulation

Consider the whole of space divided into two regions by the surface of the configuration and assume the existence of Laplacian velocity potential distributions in the two regions; i.e., Φ in the flow field and Φ_i in the blade interior. If we now apply Green's third identity to the two regions, then the total potential at a point, P, on the inside surface of the boundary can be written:

$$4\pi\Phi_P = \iint_{S-P} \left(\Phi - \Phi_i\right) \mathbf{n} \cdot \nabla\left(\frac{1}{r}\right) dS - 2\pi\left(\Phi - \Phi_i\right)_P + \iint_W \left(\Phi_U - \Phi_L\right) \mathbf{n} \cdot \nabla\left(\frac{1}{r}\right) dW$$

$$- \iint_S \frac{1}{r}\, \mathbf{n} \cdot \left(\nabla\Phi - \nabla\Phi_i\right) dS + 4\pi\Phi_{\infty_P} \qquad (1)$$

Here, r is the length of the vector from the surface element to the point, P, and S-P signifies that the point, P, is excluded from the surface integration. Equation (1) includes the contribution from the wake surface, W.

The Dirichlet boundary condition is now applied in the interior region to render a unique distribution. In principle, any potential flow can be applied. However, the flow, $\Phi_i = \Phi_\infty$, implied by Morino (28) and used by Johnson and Rubbert (25), has proven to be very reliable in practice. With this flow, Eq. (1) becomes

$$0 = \iint_{S-P} \Phi\, \mathbf{n} \cdot \nabla\left(\frac{1}{r}\right) dS - 2\pi\Phi_P + \iint_W \left(\Phi_U - \Phi_L\right) \mathbf{n} \cdot \nabla\left(\frac{1}{r}\right) dW$$

$$- \iint_S \frac{1}{r}\, \mathbf{n} \cdot \nabla\Phi\, dS \qquad (2)$$

where ϕ, the perturbation potential in the flow field, has been substituted for $\Phi - \Phi_\infty$.

The first two terms in Eq. (2) give the perturbation potential due to a distribution of normal doublets of strength, ϕ, on the configuration surface. Similarly, the third term represents a doublet distribution of strength, $\Phi_U - \Phi_L$, on the wake and the fourth term represents a source distribution of strength, $\mathbf{n} \cdot \nabla\phi$, on the configuration surface.

Equation (2) is basically the same as the formulation given by Morino (28) who used a direct application of Green's theorem in the flow field. The present approach to the problem is a special case of multi-domain formulation which has led to the more general three-dimensional method in which large regions of separated flow are modelled in a similar way to that in the CLMAX program (5), (30) and (31).

The source term in Eq. (2) can be evaluated directly from the condition of no flow penetration at the surface. The flow velocity relative to the body-fixed frame is at any instant of time

$$\mathbf{V} = \mathbf{v} + \mathbf{V}_\infty - \Omega\mathbf{h} \wedge \mathbf{R} \tag{3}$$

where the perturbation velocity is $\mathbf{v} = -\nabla\phi$, $\mathbf{h}$ is the axis of rotation, $\mathbf{V}_\infty$ and Ω are the instantaneous onset flow and angular velocity, respectively, and $\mathbf{R}$ is the relative position vector between a point on the rotation axis and a point on the surface.

For zero penetration, $\mathbf{V} \cdot \mathbf{n} = 0$. Hence,

$$\mathbf{n} \cdot \nabla\phi = \mathbf{n} \cdot \mathbf{V}_\infty - \Omega\mathbf{n} \cdot \mathbf{h} \wedge \mathbf{R},$$

and Eq. (2) becomes

$$0 = \iint_{S-P} \phi\mathbf{n} \cdot \nabla\left(\frac{1}{r}\right) dS - 2\pi\phi_p + \iint_W \left(\phi_U - \phi_L\right) \mathbf{n} \cdot \nabla\left(\frac{1}{r}\right) dW$$

$$- \iint_S \frac{1}{r}\left(\mathbf{n} \cdot \mathbf{V}_\infty - \Omega\mathbf{n} \cdot \mathbf{h} \wedge \mathbf{R}\right) dS \tag{4}$$

This is the basic equation of the method. It is solved for the unknown surface perturbation potential, ϕ, or surface doublet distribution, μ, at a number of time steps as the configuration proceeds through the motion. The wake surface is transported at the end of each step using calculated velocities of points on the wake surface. The doublet distribution, $\phi_U - \phi_L$, on each wake surface is known from solutions at earlier time steps. The unsteady Kutta condition

$$\frac{\partial \mu}{\partial t} + V \frac{\partial \mu}{\partial s} = 0 \tag{5}$$

is satisfied at points along each wake separation line at each time step.

At each time step the flow solution is determined with reference to the body-fixed frame. The incompressible pressure coefficient is, therefore, given by

$$C_p = \left(V_s^2 - V^2 + 2 \frac{\partial \mu}{\partial t} \right) / V_\infty^2 \tag{6}$$

where $\mathbf{V}_S = \Omega \mathbf{h} \wedge \mathbf{R} - \mathbf{V}_\infty$ is the instantaneous velocity of a point on the surface relative to a stationary reference frame, and $\mathbf{V}$ is given by Eq. (3).

2.3.2 Numerical Procedure

The general arrangement of the configuration is shown in Figure 4. The x,y,z coordinate system with unit vectors, **i**, **j**, **k**, is fixed relative to the configuration. For symmetrical applications, the x-z plane is regarded as the plane of symmetry.

A numerical procedure has been assembled in a time-stepping mode to obtain the unsteady pressure distribution and forces and moments. The surface of the wing is represented by planar quadrilateral panels over each of which the doublet and source distributions are assumed constant. With this assumption, the surface integrals in Eq. (4) can be performed in the closed form for each panel.

Equation (4) is then satisfied simultaneously at a point in the center of each panel. If there are N panels representing the configuration surface, Eq. (4) becomes:

$$\sum_{\substack{k=1 \\ K \neq J}}^{N} \left| \mu_K C_{JK} \right| - 2\pi\mu_J + E_J = 0; \qquad J=1,N \tag{7}$$

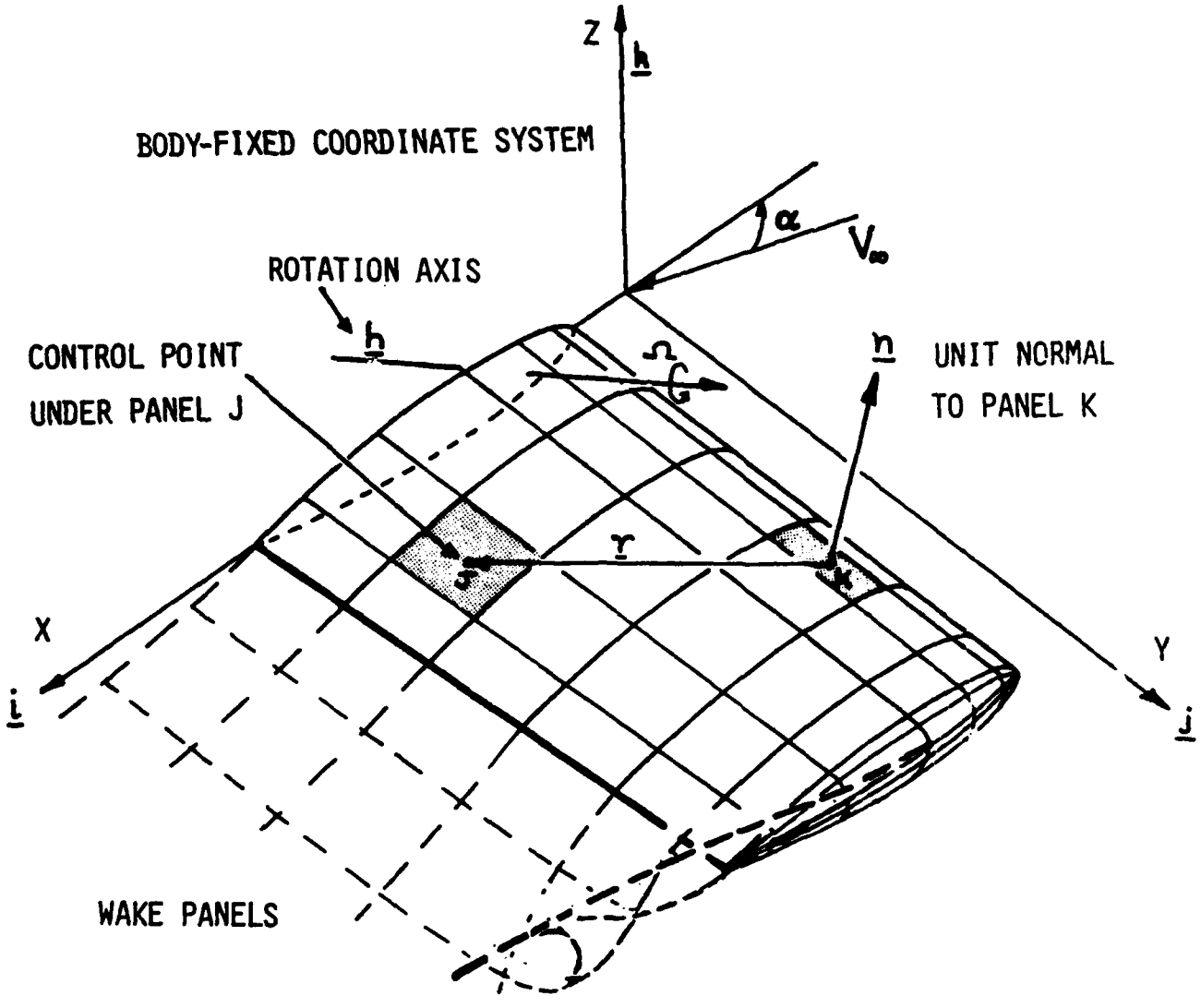

Figure 4. General Arrangement of the Configuration.

where μ_K is the unknown doublet value on Panel K. (Note: $\mu_K = \phi_K/4\pi$.)

$$E_J = \sum_{K=1}^{N_W} \left\{ \mu_{W_K} C_{JK} \right\} + \Omega\sigma_{R_J} - \mathbf{V}_\infty \cdot \sigma_{M_J}$$

where N_W, the number of panels in the wake, varies with time and Ω and $\mathbf{V}_\infty$ take their instantaneous values at each time step.

$$\sigma_{R_J} = \sum_{K=1}^{N} \left\{ \mathbf{h} \wedge \mathbf{R}_K \cdot \mathbf{n}_k \, B_{JK} \right\} /4\pi$$

is the source distribution due to rotation about the axis, $\mathbf{h}$, and

$$\sigma_{M_J} = \sum_{K=1}^{N} \left\{ \mathbf{n}_K \, B_{JK} \right\} /4\pi$$

are the components of a three-part source distribution due to the relative translation of the configuration and the onset flow. (Note: in a symmetrical case the y-component is zero.)

The quantities, B_{JK} and C_{JK}, are the velocity potential influence coefficients for the constant source and doublet distributions, respectively, on panel K acting on the control point on panel J. These include contributions from the image panel in the symmetrical case. Expressions for these influence coefficients have been given by Morino in (28) based on hyperbolic paraboloidal panels. Slightly different expressions are installed in the VSAERO code based on planar panels.

Equation (7) is solved by a direct method for $N \leq 320$ and by an iterative method for $N > 320$.

The surface pressure distribution is calculated using Eq. (6). The surface gradient of μ is evaluated on each panel by differentiating a two-way parabolic fit through the doublet values on the panel and its four immediate neighbors. At the separation lines a simple differencing is applied for the gradients approaching the separation line.

The gradient of ϕ with respect to time is evaluated by central differencing over two time steps; i.e.,

$$\frac{\partial \phi}{\partial t}^{t-\Delta t} = \left(\phi^t - \phi^{t-2\Delta t} \right) /2\Delta t.$$

For harmonic motions the real and imaginary pressure are obtained by Fourier analysis for the first harmonic based on solutions over a complete cycle. The calculations start with incidence α_o and a regular (i.e., steady) wake. Two iterations are performed to render the wake force free. An oscillatory doublet component based on a linearized solution is then superimposed along each wake line before starting the time-step model. Time-step calculations proceed over a half cycle before applying the Fourier analysis.

At each time step a new panel is formed at the head of each column of wake panels and all the existing wake panel corner points are convected downstream at the local velocity. Each wake panel keeps the doublet value it received at the time it was formed. This doublet value is based on the conditions at the separation line and satisfies Eq. (5). It is assumed that the shedding occurs at constant vorticity over the time interval, t. In this way the doublet strength, $\mu_W^{t+\Delta t}$, on the new wake panel is related to the strength, μ_W^{t}, of the previous wake panel at the separation line by

$$\mu_W^{t+\Delta t} = 2\mu_T^{t} - \mu_W^{t},$$

where μ_T^{t} is the resultant doublet value at the separation line.

2.4 Unsteady Separated Flow

The combined code for separated flow modeling in the unsteady case requires a more sophisticated treatment of the free-shear layer model than was used for the steady case. Velocities are still calculated at a set of points along each free sheet, but in the unsteady case we now transport these points (and their associated doublet value) along the calculated velocity vectors for a small time interval, Δt. In this way as time progresses, a dynamic wake model is generated. At each step a new piece of free sheet is shed from the calculated separation point; the strength and size of this new segment is determined by the local upstream velocity condition. The location of the separation--calculated using an unsteady boundary layer code, see the next section--can now move with time.

It is convenient to regard the local vorticity (i.e., doublet gradient on the free vortex sheets in two components; a streamwise component and a cross-flow component. The streamwise component is already force free and is related to the spanwise rate of shedding of circulation from the wing. The cross-flow vorticity component is associated with direct dumping of bound

circulation from the separation line and must be transported with the local flow velocity in order to be force free. This cross-flow vorticity component--which was assumed constant with streamwise distance in the steady case--now varies along each streamline on the free sheets for two reasons: first, the vorticity value being convected onto the free sheet at each separation point is varying in time because of varying onset flow conditions and because of the changing separation locations; secondly, stretching by the entire configuration of solid surfaces and free wake sheets. This stretching of the doublet distribution carried by the free sheets yields varying vorticity values when the doublet gradient is evaluated. In this way the free sheets can become highly distorted and centers of vortex roll-up may form. Special treatment of the sheets is therefore essential if numerical stability is to be maintained. Two routines are being evaluated in this work but they have not been fully implemented at this time.

(i) Vortex Amalgamation

To cater for vortex roll-up in a reasonable manner it is essential to include a vortex core model in which integrated vorticity is accumulated rather than to follow a detailed calculation of multiple turns of a vortex spiral. An amalgamation scheme similar to that of Moore (39) is being used. When the angle between neighboring segments representing a sheet exceeds a specified angle, the segment end points are merged to a new location at the centroid of their combined circulation. A number of such cores are allowed in the new routine to deal with complex motions. A viscous core expression can be applied to each vortex core when computing the field velocities.

(ii) Redistribution

Having performed the vortex-core amalgamation calculation along each free sheet the points defining the intermediate free sheets are redistributed with equal spacing in a manner similar to Fink and Soh (40) and Sarpkaya and Schoaff (41). Portions of the sheet between amalgamated cores are treated independently here, Figure 5. This treatment, which is applied to both the sheet geometry and its doublet distribution, uses a biquadratic interpolation scheme based on surface distance along the sheet.

This routine should help stabilize the numerical calculations, especially in the initial part of each sheet when the separation location is varying with time. In the three-dimensional case the redistribution scheme is being arranged along the calculated mean streamlines in the wake sheets. This causes some difficulty if amalgamation is not proceeding uniformly along all lines on a sheet.

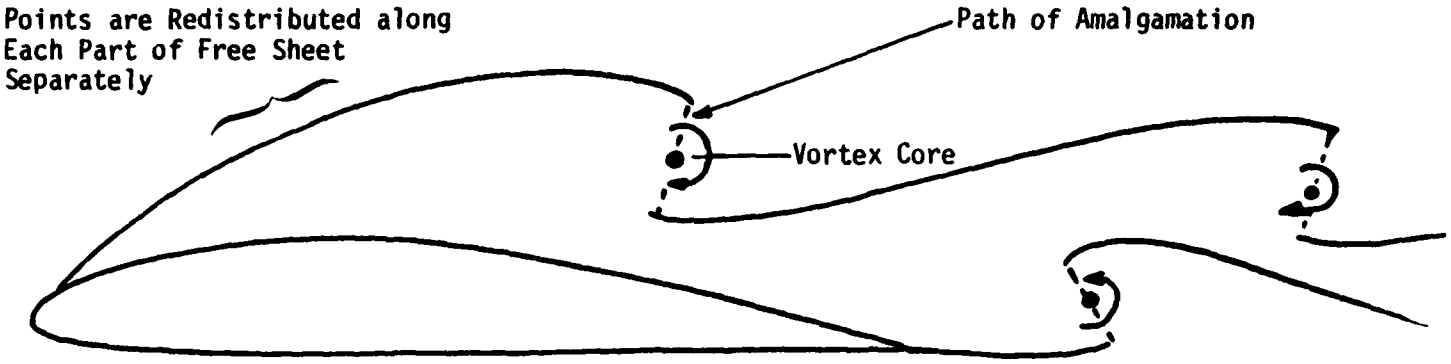

Figure 5. Illustration of Multiple Vortex Core Amalgamation and Redistribution Scheme.

2.5 Calculations

As the routines are being developed, preliminary calculations are being performed to check the basic operation of the code. Figure 6 shows the growth of indicial lift and circulation for a NACA 0012 impulsively started from rest at an angle of attack of .1 rad. The curves are compared with Wagner's function for indicial lift and R.T. Jones indicial circulation for a flat plate. The initial calculations, which used 31 panels around the section, are in good agreement and indicate a slightly higher trend which is consistent with a higher steady state circulation for the thickness case.

Some recent refinements developed in the two-dimensional pilot code have significantly reduced the computing requirement of these time-stepping calculations. For example, Figure 7 shows the effect on indicial lift of varying the number of time steps in the Wagner problem and demonstrates a rapid convergence.

The procedure has been tested also for the harmonic oscillation case. Earlier calculations required 80 time steps per cycle for a NACA 0012 oscillating in pitch about the quarter chord. These compared favorably with the Theodorsen flat plate function over a range of reduced frequency, Figure 8. The new calculations are also in good agreement but were performed with only 16 time steps per cycle. Figure 9 shows the computed results. C_L versus time, using only 4 time steps per cycle. This is in remarkably good agreement with the 16 and also 32 time-step/cycle solutions, demonstrating an extremely good convergence characteristic.

Time-stepping calculations have also been performed for cases with prescribed extensive separations. The purpose of these calculations was to check the basic unsteady circulation shedding model in the potential flow code. For the first set of tests, the wake panels were simply transported at the onset flow velocity after the initial growth as determined from the surface conditions at separation. Several triangular shapes were considered, each starting impulsively from rest and proceeding forward over 10 time steps for a total time of $\tau = \tau U_\infty/h = 3.0$, where h is the triangle base height. Separation was prescribed at the corners. Figure 10(a) shows the computed history of the drag coefficient from pressure integration for a 60 degree triangle with blunt face forward. A total of 40 panels was used to represent the triangle surface. The calculation was repeated in the presence of wind tunnel walls (also panelled) with a 10% blockage ratio. The indicated blockage correction is somewhat lower than that given by standard techniques. Figure 10(b) compares the computed pressure distributions for this triangle in and out of the tunnel. This "base" pressure has only a small variation and is quite close to experimental measurements. Figure 11 shows a summary of computed drag coefficient versus triangle semi-apex angle. The calculated values are slightly

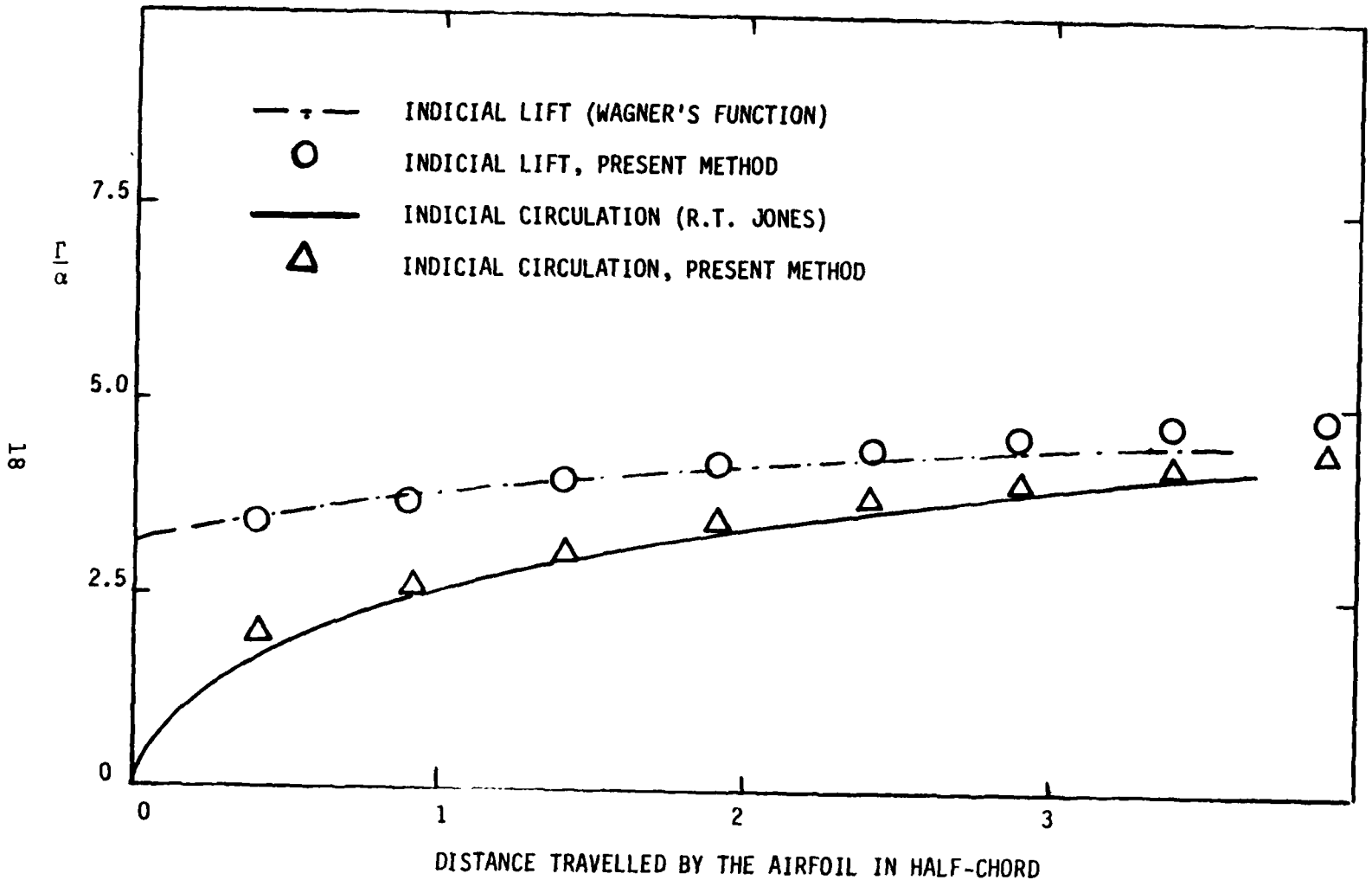

Figure 6. Indicial Lift and Circulation for an Impulsively Started Two-Dimensional Flat Plate.

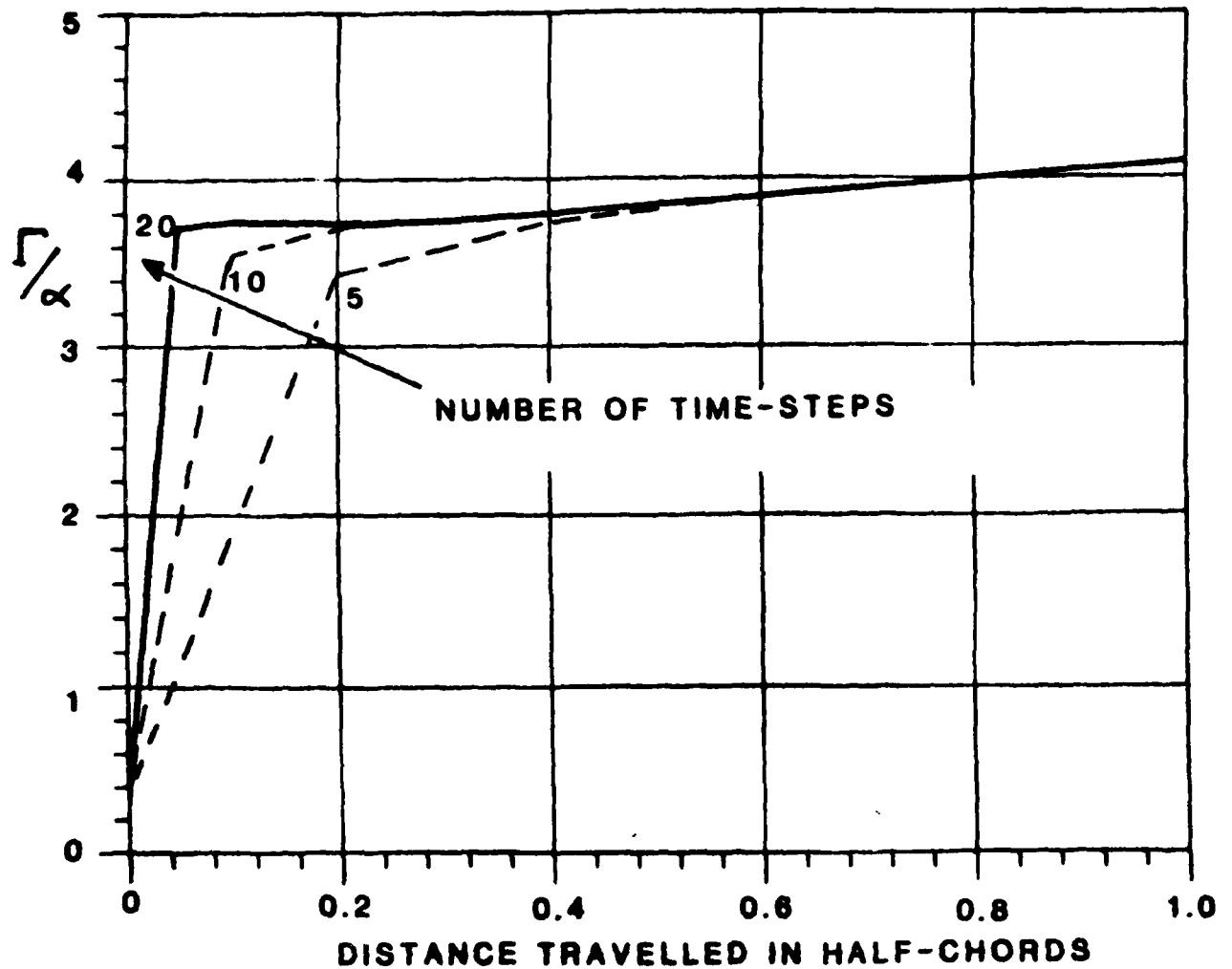

Figure 7. INDICIAL LIFT FOR AN IMPULSIVELY STARTED NACA 0012 OSCAIR CALCULATIONS

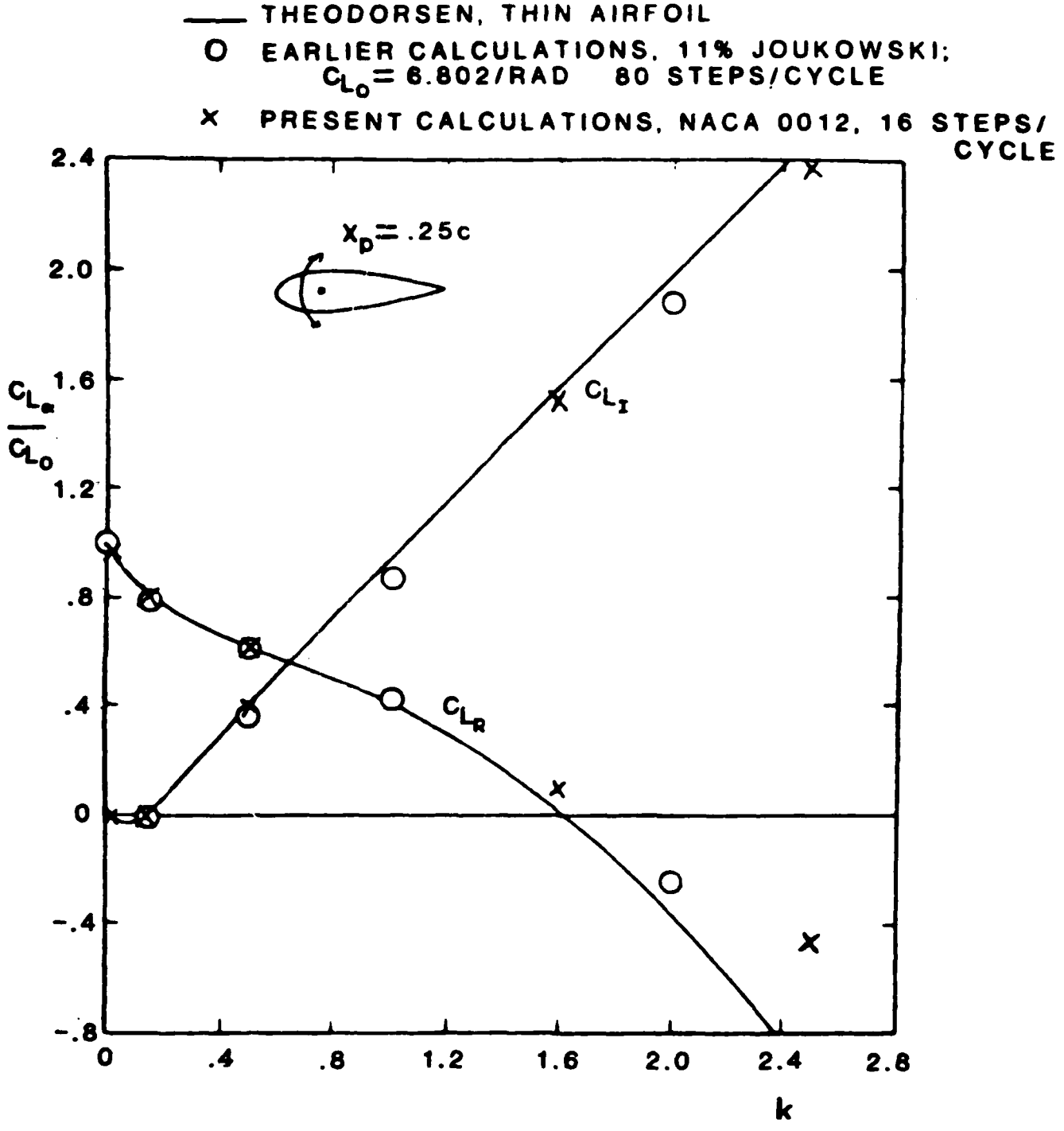

Figure 8. Comparison of Real and Imaginary Lifts as a Function of Reduced Frequency, $\alpha = 1° \sin kt$.

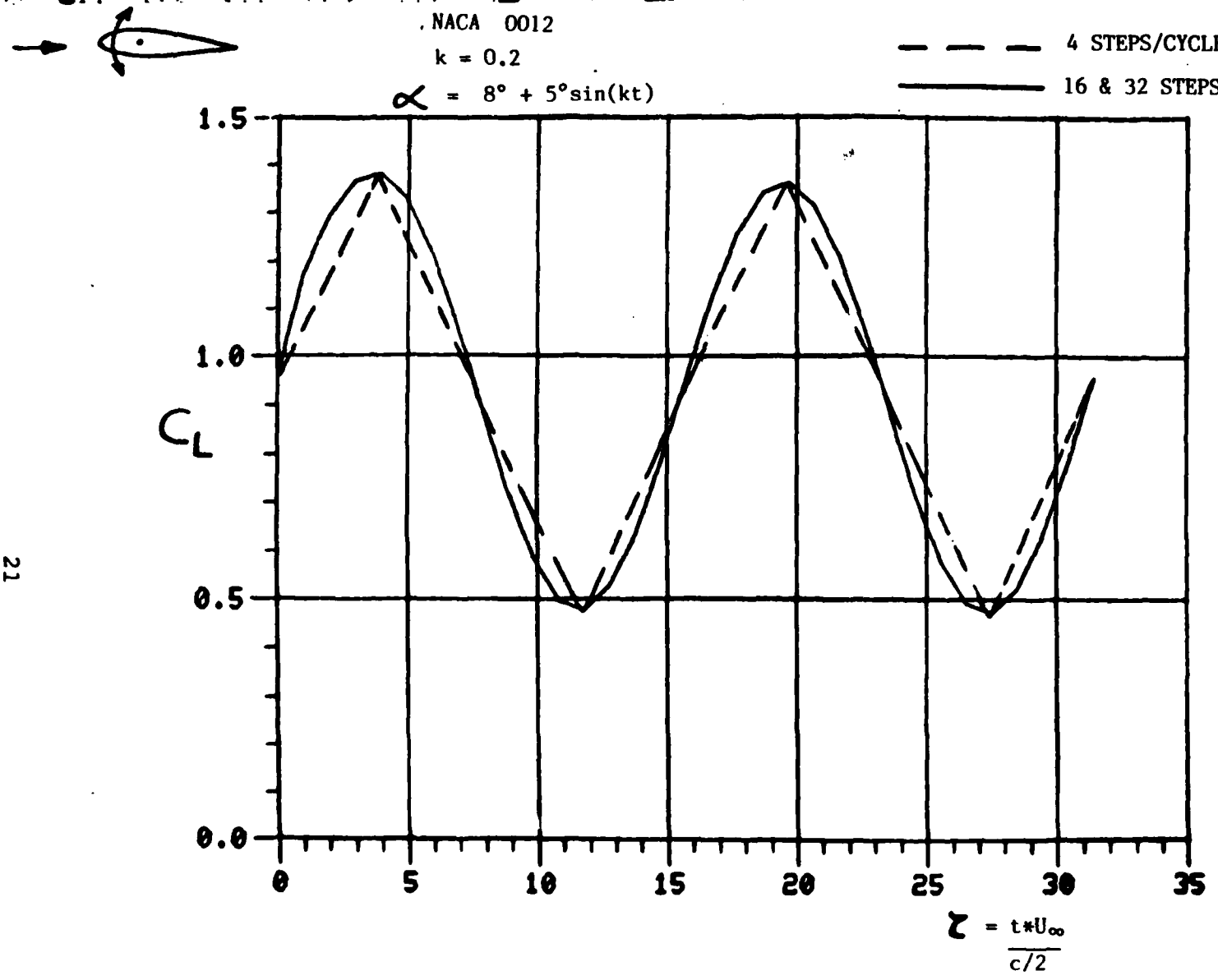

Figure 9. CALCULATED C_L ~TIME FOR A NACA 0012 OSCILLATING IN PITCH ABOUT 1/4 CHORD

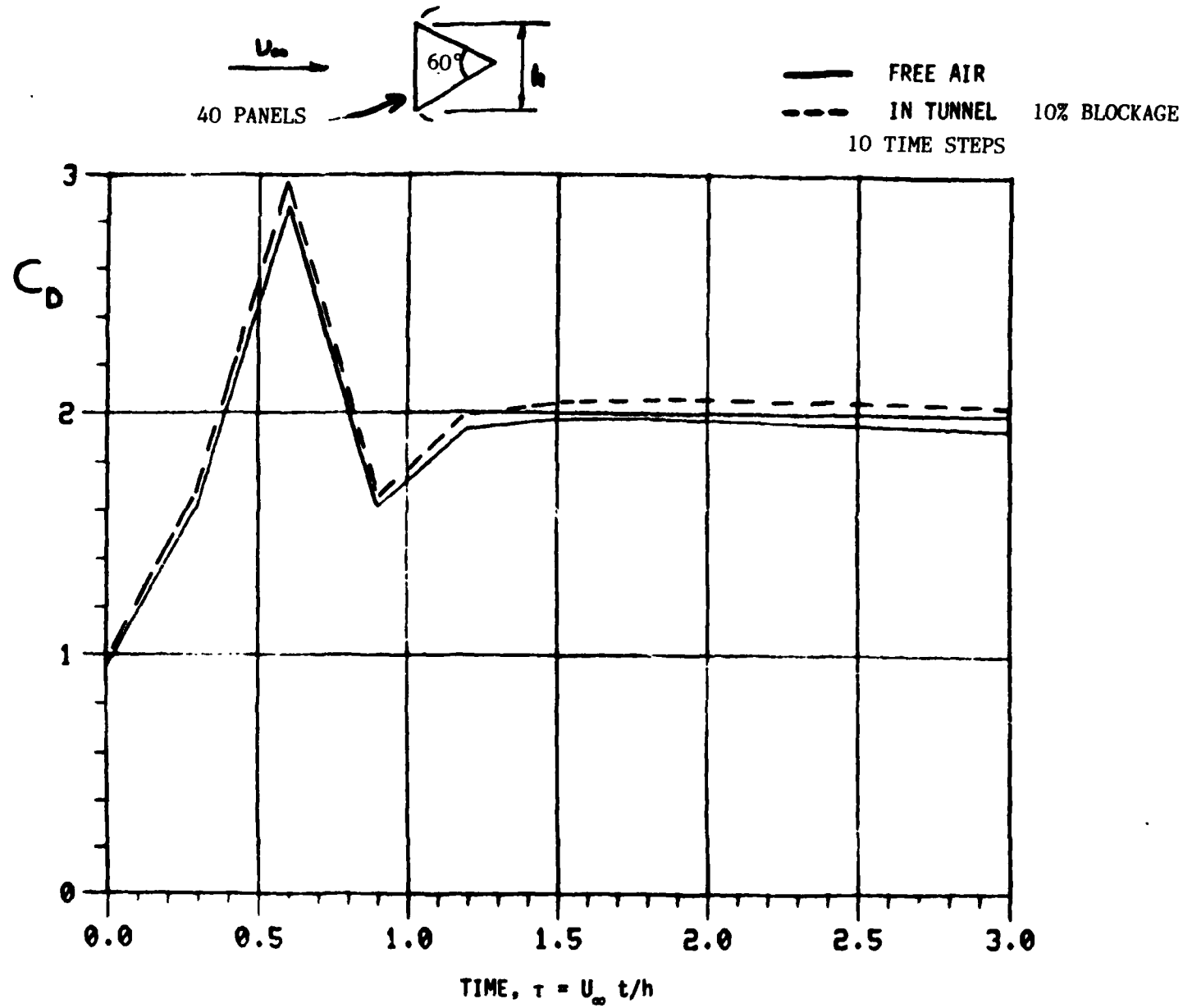

Figure 10(a). **CALCULATED DRAG HISTORY FOR A 60° WEDGE STARTED IMPULSIVELY FROM REST**

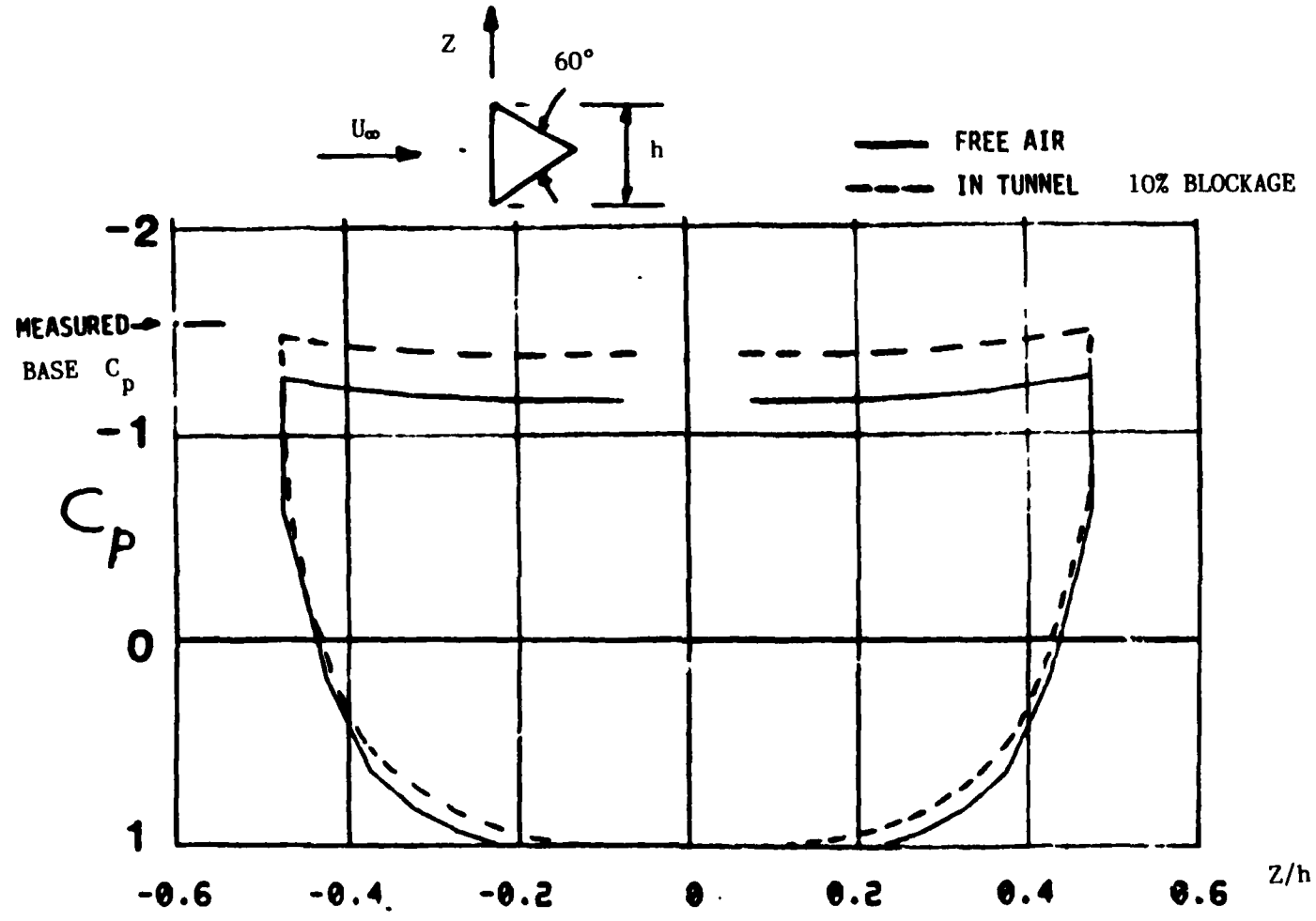

Figure 10(b).

CALCULATED PRESSURE DISTRIBUTION FOR A 60° WEDGE STARTED IMPULSIVELY FROM REST: $\tau = U_\infty t/h = 3.0$

high in relation to the experimental data collected from several sources by Hoerner in Fluid Dynamics.

One further case was run for the 60 degree, apex-forward triangle in free air with the full wake velocity calculation routine turned on but without the amalgamation and redistribution schemes at this stage. The calculated C_D for this case falls below the experimental value, Figure 11. A series of computed wake shapes is shown in Figure 12. These are samples from a total of 40 time-step calculations. The total computing time for this case was 195 seconds on a PRIME 550 minicomputer--this is equivalent to less than 2 seconds of CRAY time. The solution should benefit from the numerical damping provided by the amalgamation and redistribution schemes described earlier.

Finally, a test calculation was performed for a NACA 0012 section in a state of pitch from 10 degrees to 30 degrees with $\dot{\alpha}c/2U_\infty = .175$. The calculation used 30 panels and 10 time steps. Separation points were prescribed and the motion was started impulsively from rest.

Figure 13(a) shows a sample of the computed wake shapes and demonstrates a reasonable numerical behavior. Sample pressure distributions are shown in Figure 13(b). The passage of the leading-edge vortex is clearly shown. This is associated with a local region of reversed flow. These are preliminary test calculations aimed at exploring the numerical behavior of the calculation procedure and potential flow model. Future cases will include the coupled boundary layer calculation for predicting the separation point. At that time the calculated results will be compared with experimental data.

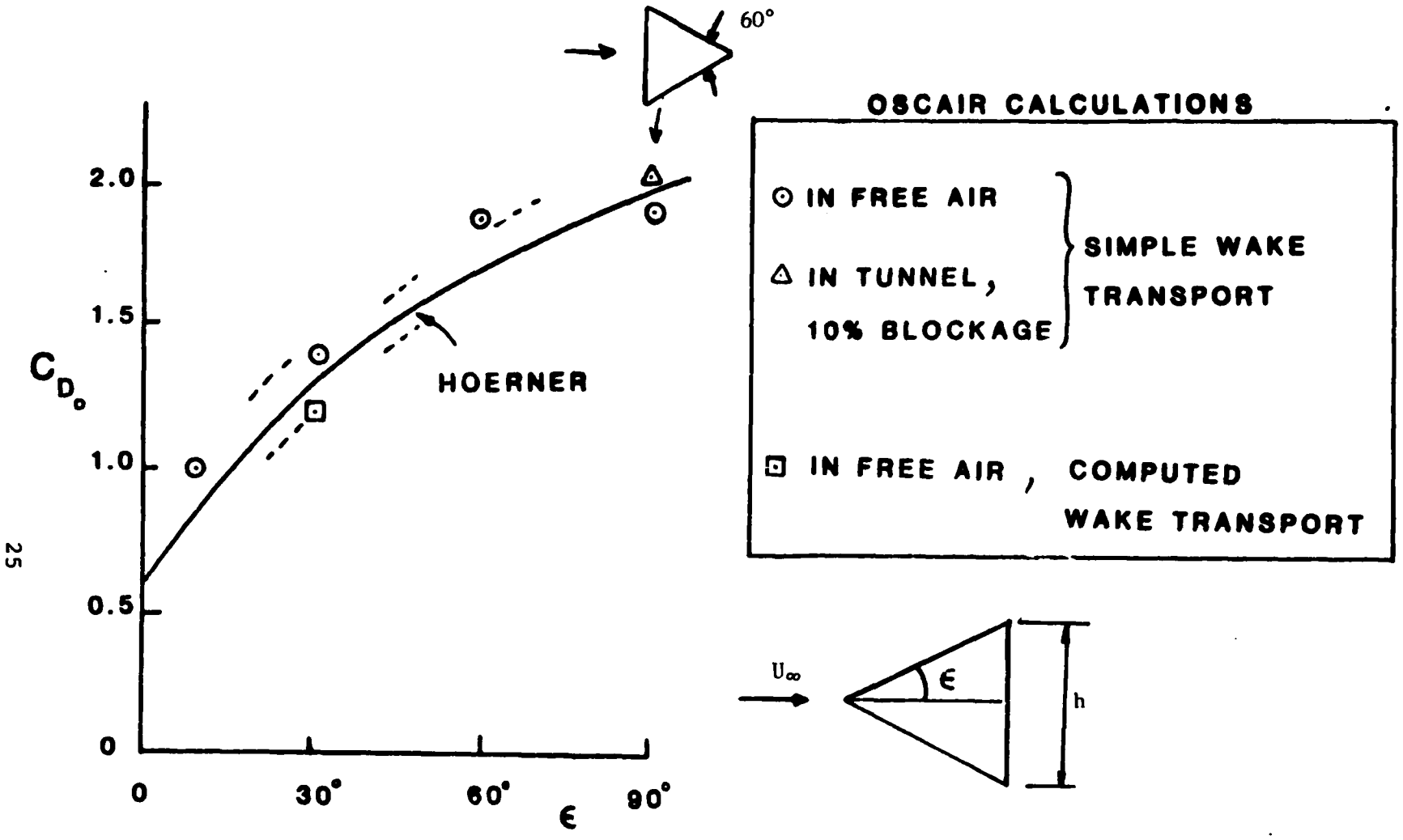

Figure 11. Calculated Drag Coefficient of Two-Dimensional Wedges as Function of Semi-Apex Angle.

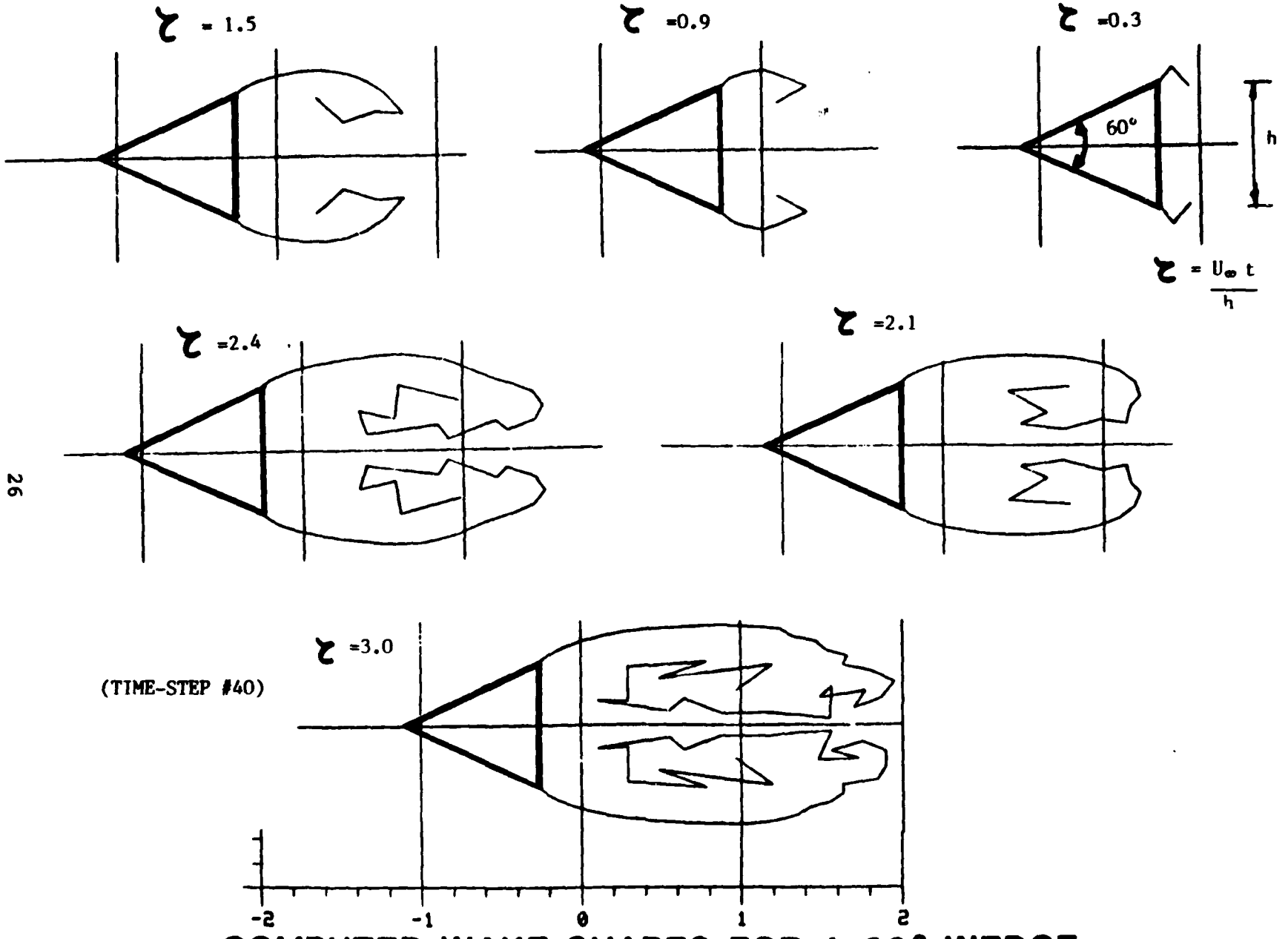

Figure 12. COMPUTED WAKE SHAPES FOR A 60° WEDGE STARTED IMPULSIVELY FROM REST

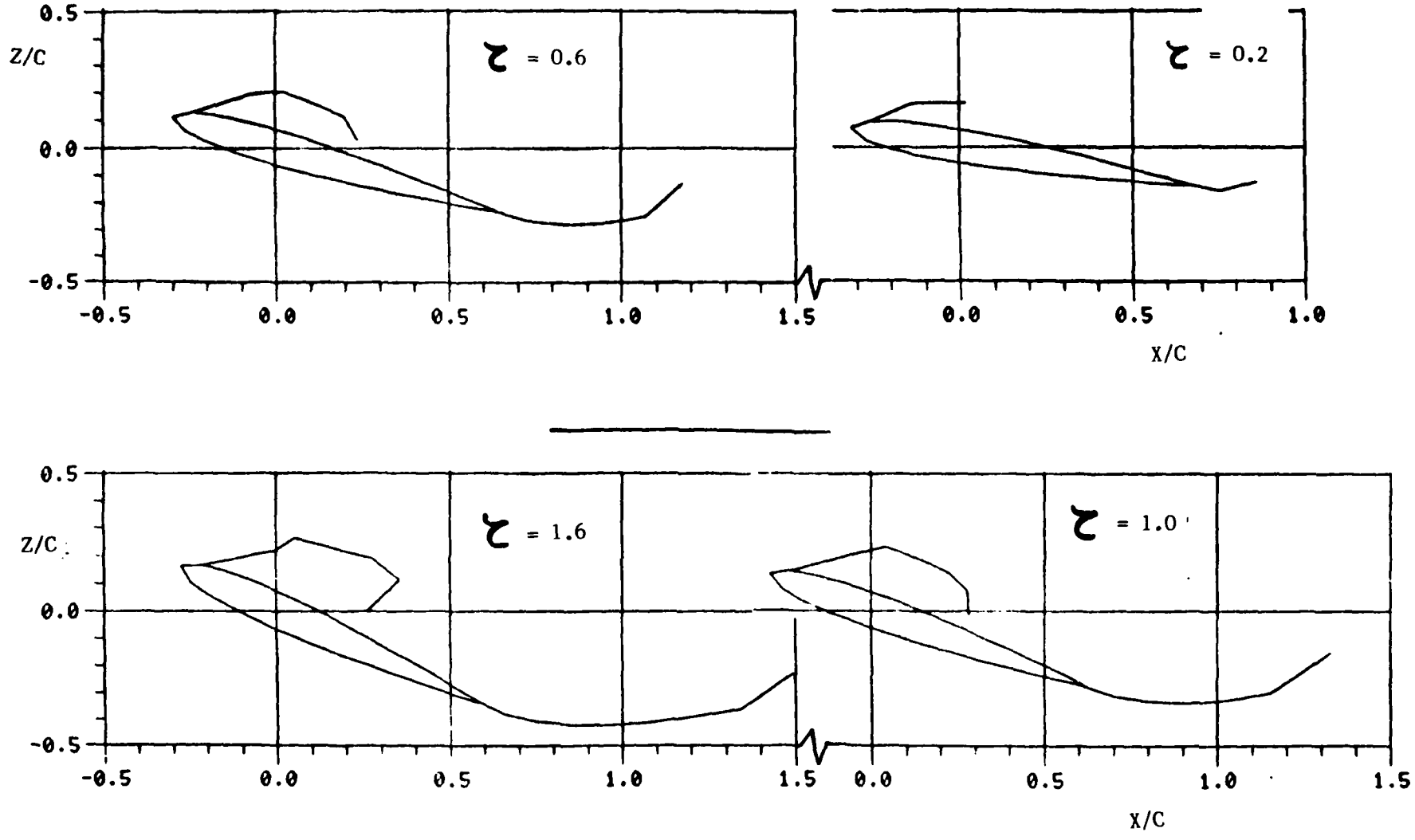

Figure 13(a). **NACA 0012 STARTING IMPULSIVELY FROM REST PITCHING FROM 10° TO 30° : $\dot{\alpha}\, C/2U_\infty = 0.175$**

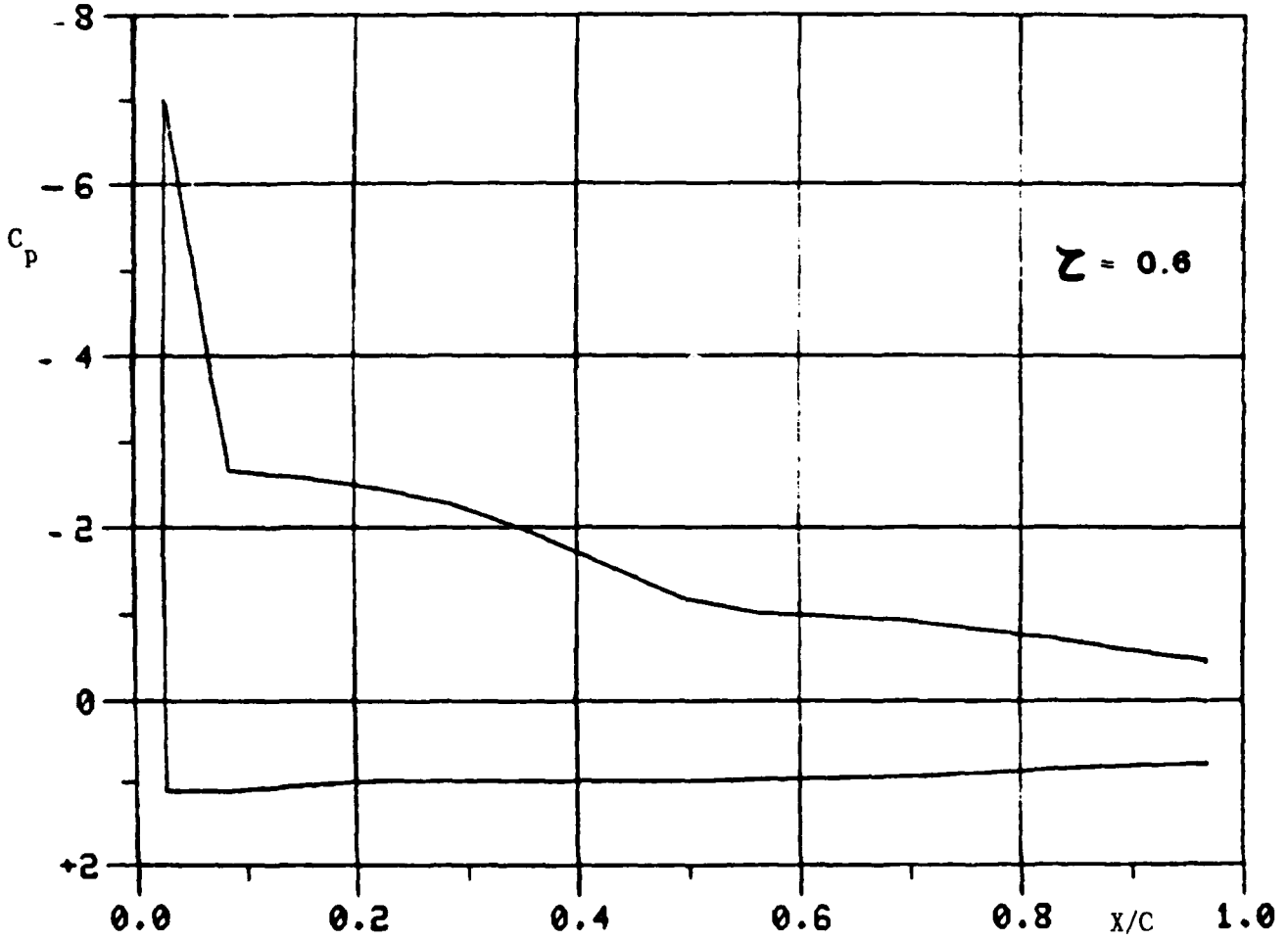

NACA 0012 STARTING IMPULSIVELY FROM REST PITCHING FROM 10° TO 30°: $\dot{\alpha}\, C/2U_\infty = 0.175$

Figure 13(b) (i).

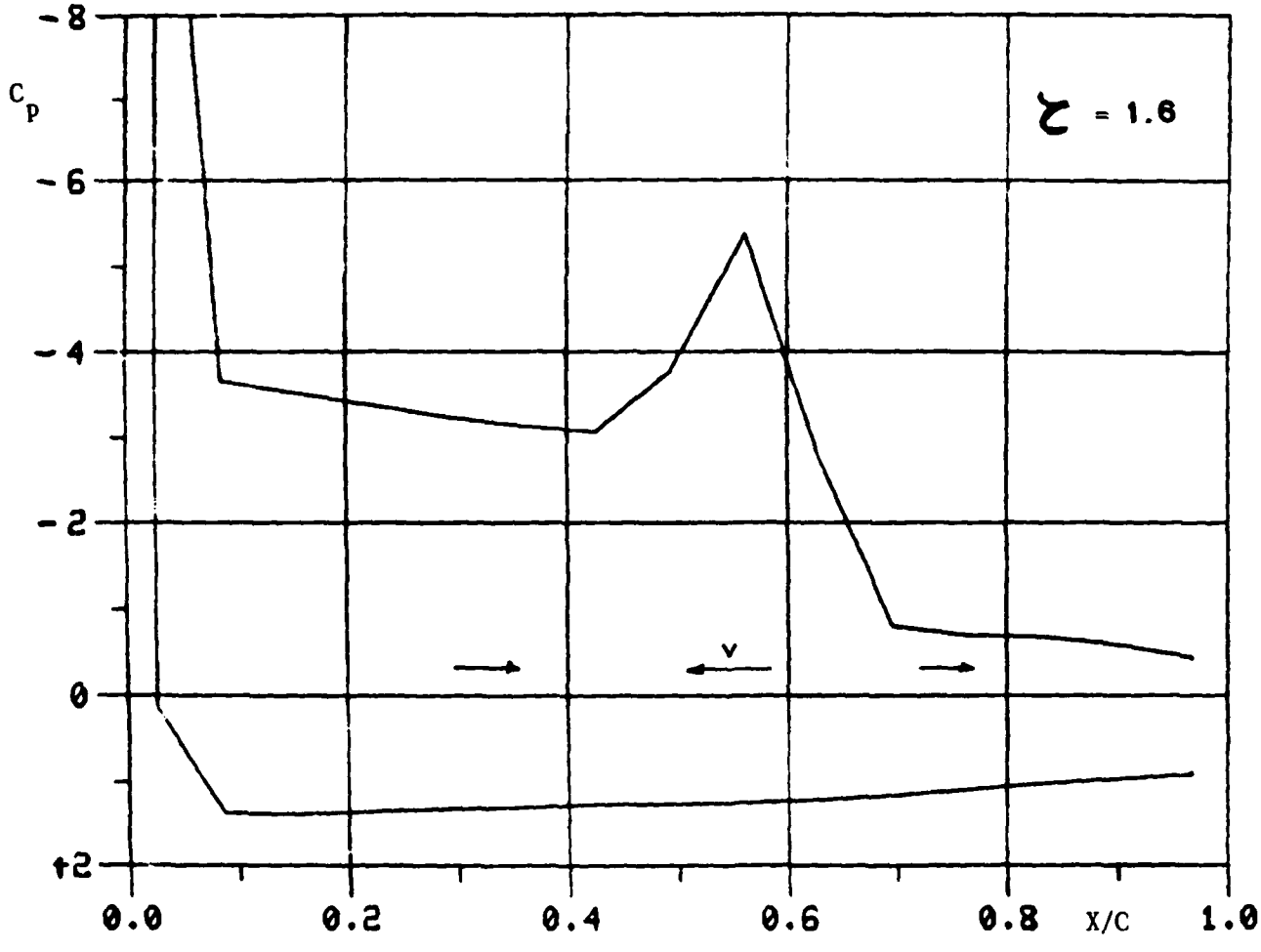

NACA 0012 STARTING IMPULSIVELY FROM REST PITCHING FROM 10° TO 30°: $\dot{\alpha}\, C/2U_\infty = 0.175$

Figure 13(b) (ii).

3.0 BOUNDARY LAYER CALCULATION METHOD

Curle's original method has been modified to calculate the unsteady boundary layer development. This is achieved by solving the unsteady momentum integral equation using a Runge-Kutta method. The turbulent boundary layer method is based on the unsteady momentum integral equation as in the laminar boundary layer method. Cousteix's entrainment relationship (43) and Lyrio/Ferziger's skin friction relationship (44) are used for closure. The details of the methods are described in the following sections.

3.1 Laminar Boundary Layer Method

$$\frac{\partial \theta}{\partial x} + \theta \frac{H + 2}{U_e} \frac{\partial U_e}{\partial x} + \frac{1}{U_e^2} \frac{\partial}{\partial t}(\delta^* U_e) = \frac{C_f}{2} \tag{8}$$

or

$$\frac{\partial \theta}{\partial x} = - \frac{1}{U_e} \frac{\partial \delta^*}{\partial t} + \frac{C_f}{2} - \frac{\theta(H + 2)}{U_e} \frac{\partial U_e}{\partial x} - \frac{\delta^*}{U_e^2} \frac{\partial U_e}{\partial t} \tag{9}$$

This is a first-order differential equation for V and can be solved for θ if additional relationships for θ, C_f and δ^* are given. In Curle's steady boundary layer procedure, these relationships are expressed as

$$C_f = 2 \cdot \ell / R_\theta \tag{10}$$

$$L = 2[\ell - K(H + 2)] \tag{11}$$

where

L, ℓ = functions of μ and K

$$K = \theta^2 / \nu (dU_e/dx) \tag{12}$$

$$\mu = K^2 U_e U_e'' / U_e'^2$$

Calculation begins at the stagnation point and K takes the starting value, $K_o = 0.0855$. The inital momentum thickness, θ_o, is

$$\theta_o = (0.0855\nu/(dU_e/d))^{\frac{1}{2}} \tag{13}$$

3.2 Turbulent Boundary Layer Methods

For unsteady turbulent boundary layers, the momentum integral equation and the entrainment equation are given by:

$$\frac{\partial\theta}{\partial x} + \theta\frac{H+2}{U_e}\frac{\theta U_e}{\partial x} + \frac{1}{U_e}\frac{\partial}{\partial t}(\delta^* U_e) = \frac{C_f}{2} \tag{14}$$

$$\frac{1}{U_e}\frac{\partial}{\partial x}[U_e(\delta - \delta^*)] = C_E \tag{15}$$

where

$$C_E = \frac{\partial\delta}{\partial x} - \frac{V_e}{U_e}. \tag{16}$$

Equations (14) and (15) have five unknowns; i.e., C_E, C_f, δ, θ, and δ^*, and the system needs additional relationships for closure.

For the skin friction, a new correlation of Lyrio et al. (44) is used:

$$\frac{C_f}{2} = .051|1 - 2\Lambda|^{1.732}(\Lambda/Re^*)^{0.268}\,\mathrm{sgn}(1 - 2\Lambda) \tag{17}$$

where

$$\frac{H-1}{H} = 1.5\Lambda + 0.279V_T + 0.321\,V_T^2/\Lambda \tag{18}$$

$$\Lambda = \frac{\delta^*}{\delta} \tag{19}$$

$$V_T = \frac{1}{k}\sqrt{\frac{|\tau_w|}{\rho U_\infty^2}}\,\mathrm{sgn}(\tau_w) \tag{20}$$

and $k = 0.41$ is the von Karman constant.

The similarity solutions have shown that the entrainment coefficient, C_E, can be expressed as

$$C_E = C_{E_S} - \frac{1}{U_e} \frac{\partial \delta}{\partial t} \tag{21}$$

where C_{E_S} is the entrainment coefficient for the steady case as given by:

$$C_{E_S} = \sqrt{\frac{C_f}{2}} (0.074G - 1.0957/G) \tag{22}$$

Substitution of Eq. (21) into Eqs. (14) and (15) and the introduction of $H^* = (\delta - \delta^*)/\theta$ give

$$\frac{1}{U_e} \frac{\partial \delta^*}{\partial t} + \frac{\partial \theta}{\partial x} = B_1 \tag{23}$$

$$H^{*\prime} \frac{\partial \delta^*}{\partial x} + \frac{1+H^{*\prime}}{U_e} \frac{\partial \delta^*}{\partial t} + (H^* - HH^{*\prime}) \frac{\partial \theta}{\partial x} + \frac{H^* - HH^{*\prime}}{U_e} \frac{\partial \theta}{\partial t} = B_2 \tag{24}$$

with

$$B_1 = \frac{C_f}{2} - \frac{\theta(H + 2)}{U_e} \frac{\partial U_e}{\partial x} - \frac{\delta^*}{U_e^2} \frac{\partial U_e}{\partial t}$$

$$B_2 = C_{E_S} - \frac{\delta - \delta^*}{U_e} \frac{\partial U_e}{\partial x}$$

Equations (23) and (24) constitute a system of first-order hyperbolic partial differential equations for δ^* and θ. The characteristic equation of the second degree for the parameter, $\lambda = \frac{dx}{U_e dt}$:

$$\lambda^2(H^* - HH^{*\prime}) + \lambda[1 - H^* + H^{*\prime}(1 + H)] - H^{*\prime} = 0 \tag{25}$$

Equations (23) and (24) can be solved in various ways. Initial conditions at t = 5o and boundary conditions at the stagnation point (t > 0) are sufficient to determine a solution in the region where the flow is attached; i.e., $\lambda_2 > 0$. In the present paper, the time derivatives are treated as forcing terms and the integration is performed in the x-direction using a Runge-Kutta method.

The boundary layer procedure has been tested against experiments and the calculations of other investigators. The results are shown in Figures 14 and 15. Figure 14(a), (b), and (c) shows the mean quantities (momentun thickness, skin friction and shape factor) for the experiment conducted by Cousteix (45) on a flat plate. The main free stream velocity is 22 m/sec and the motion is harmonic with respect to time with the frequency of 38 hz. The present calculation (solid line) agrees very well with the calculation by Cousteix and the correlation with experiment is also very good.

Figure 15 shows the comparison with the calculation of Nash et al. (46) for a monotonically time-varying flow on a flat plate. The present calculation predicts the separation at the end of the plate when wt = 0.682 as in the Nash et al. calculation. the overall results are in good agreement with their calculation.

These test calculations have shown that the current boundary layer procedure is capable of predicting the unsteady boundary layer development and it should be adequate for analyzing dynamic stall problems.

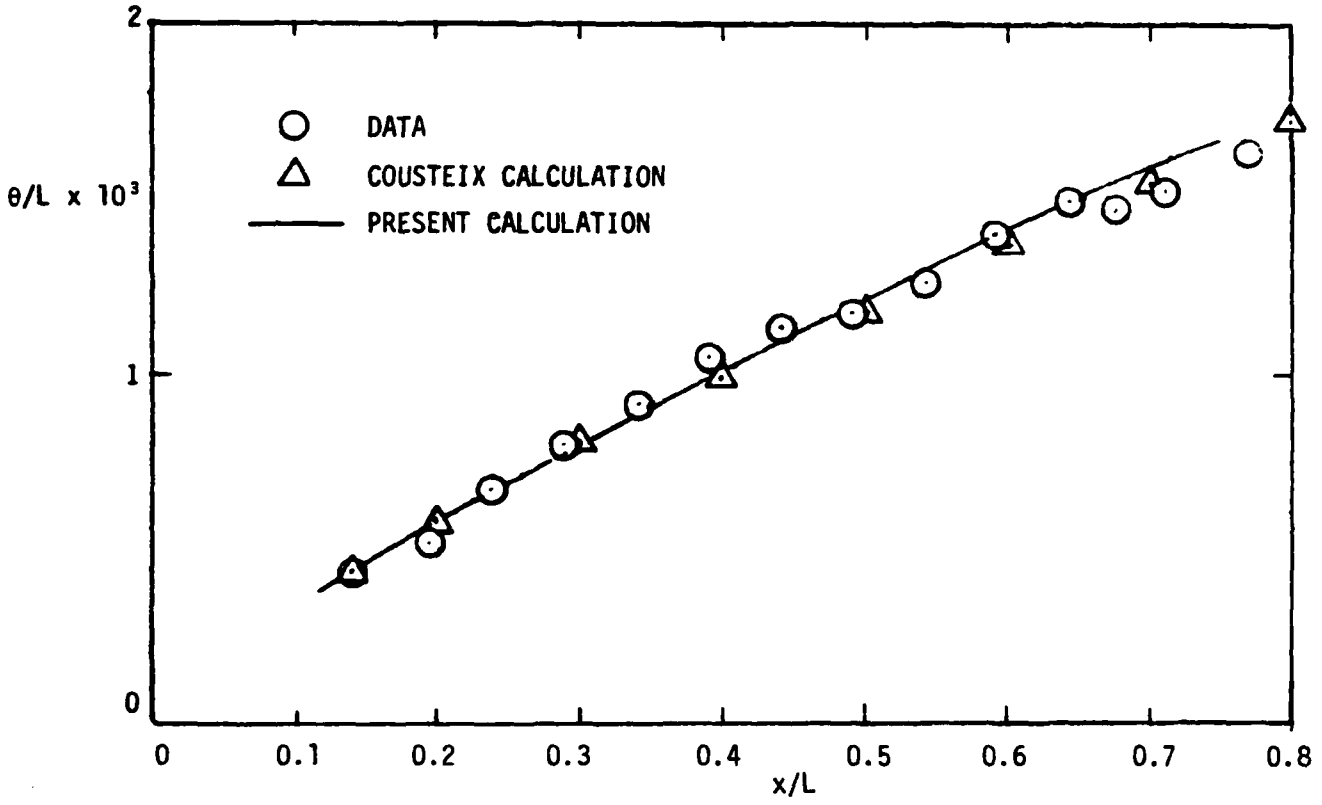

Figure 14(a). Mean Momentum Thickness; $\overline{U}_o$ = 22 m/sec, $U_e = \overline{U}_o$ (1 + 0.15 cos ωT), F = 38 Hz.

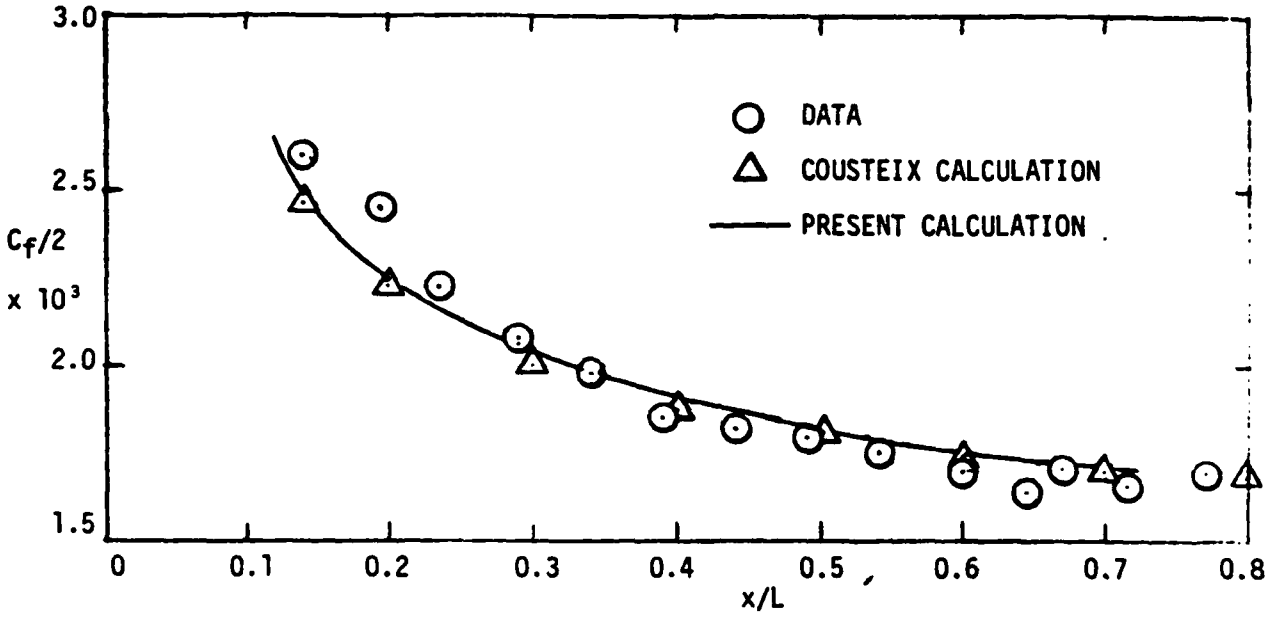

Figure 14(b). Mean Skin Friction Coefficient.

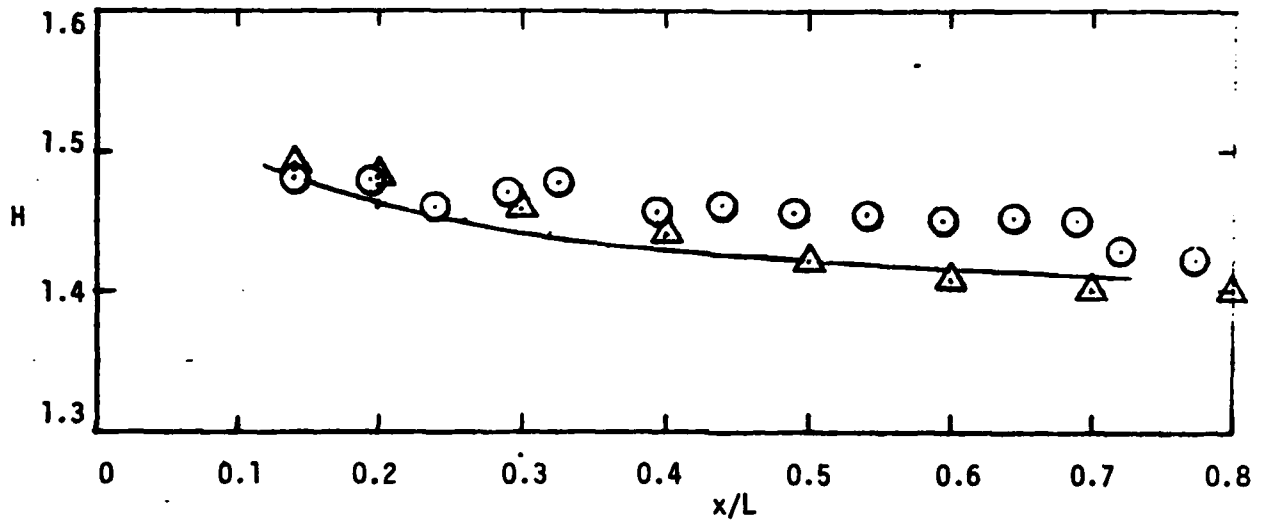

Figure 14(c). Mean Shape Factor.

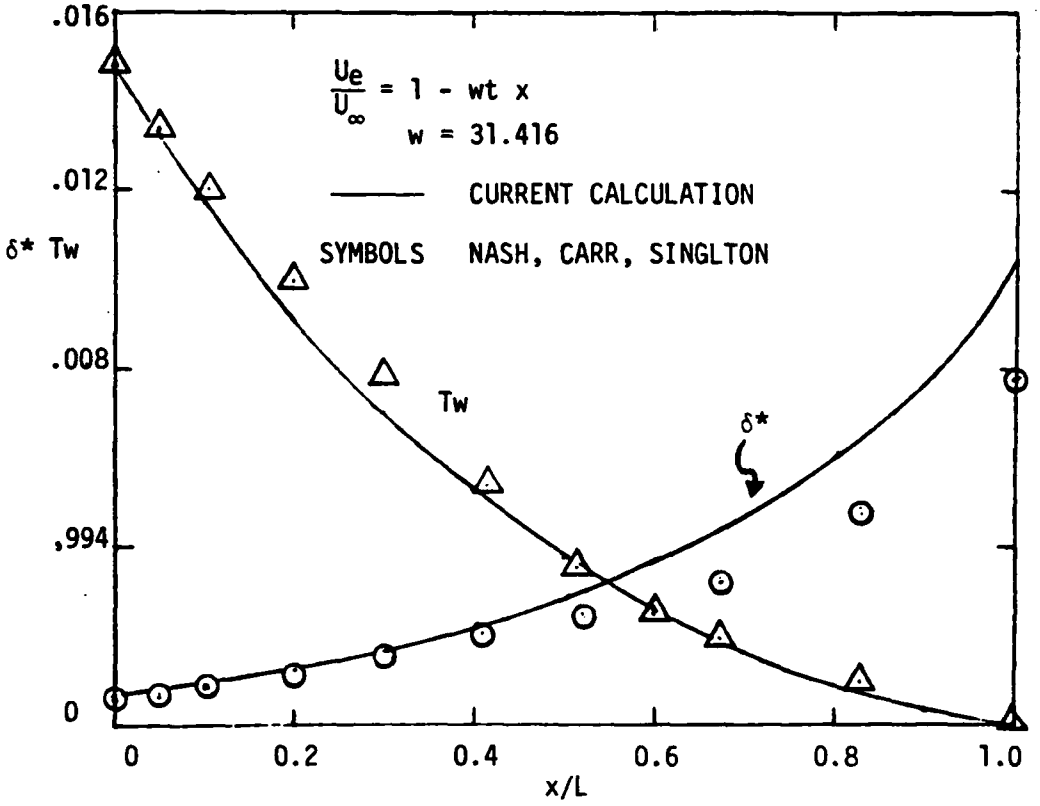

Figure 15. Wall Shear Stress and Displacement Thickness Distribution at wt = 0.682.

4.0 COMPLETE PROCEDURE

The complete procedure coupling the unsteady time-stepping potential flow panel method, the extensive separation wake model and the unsteady boundary layer code has been assembled in the pilot code for a system checkout prior to forming the three-dimensional version. The flow diagram for the procedure is shown in Figure 16. At this time the unsteady boundary layer code is called at each time step and is fed by unsteady derivatives from the potential flow calculation.

An experimental data case from (3) was run and the computed lift variation with α compared with the measured data in Figure 17. The airfoil is a NACA 0012 and is oscillating in pitch about the quarter-chord line with $\alpha = 8.1° + 4.9° \sin(0.2t)$; i.e., below the dynamic stall onset. Reynolds number was 4×10^6. This reduced frequency condition is very close to the changeover from a lead to a lag situation and so there is only a small difference between the upswing and downswing curves.

A preliminary calculation was performed for a NACA 0012 section oscillating in pitch about the quarter-chord with $\alpha = 10° \sin(2t)$. Figure 18 shows the predicted history of the separation location superimposed on the α history. The most forward separation reached .2 x/c with a phase lag of about 17°.

The above calculation was performed with just the trailing-edge wake. Calculations are now proceeding with linear pitch-up with a second (upper surface) separated wake. Experimental measurements of airfoils undergoing constant rate pitch-up motions have been taken at the Frank J. Seiler Research Laboratory (47). Three cases are considered briefly here for correlation purposes. In these cases the airfoil is pitched up from $\alpha = 0$ to approximately 1 radian at a constant pitch rate and then held at constant angle of attack. Three pitch rates are considered with normalized pitch rates, $k (= \dot{\alpha}c/2U_\infty)$ of .047, .089 and .133. Figures 19 (a), (b), and (c), respectively, show the comparison between calculated and measured $C_L \sim \alpha$ and $C_D \sim \alpha$ characteristics for these cases. For the low pitch rate, $k = 0.047$, the comparison is very good up to about 30° but then deteriorates. The calculated C_L remains fairly constant with α until the pitch rate drops to zero while the experimental curve falls markedly. The calculated rise in drag with α has a steady rate in the 30° to 60° range while the experimental measurements include a substantial increment above this rate peaking at about $\alpha = 40°$. There is a good agreement between calculated and measured lift and drag values for the final "steady state" conditions at $\alpha = 60°$.

One possible reason for the departure of the calculated lift and drag in the latter part of the pitch-up phase is the modeling of the leading-edge vortex roll-up. The amalgamation and redistribution schemes that were installed to stabilize the dynamic wake calculations are not performing in a consistent manner at

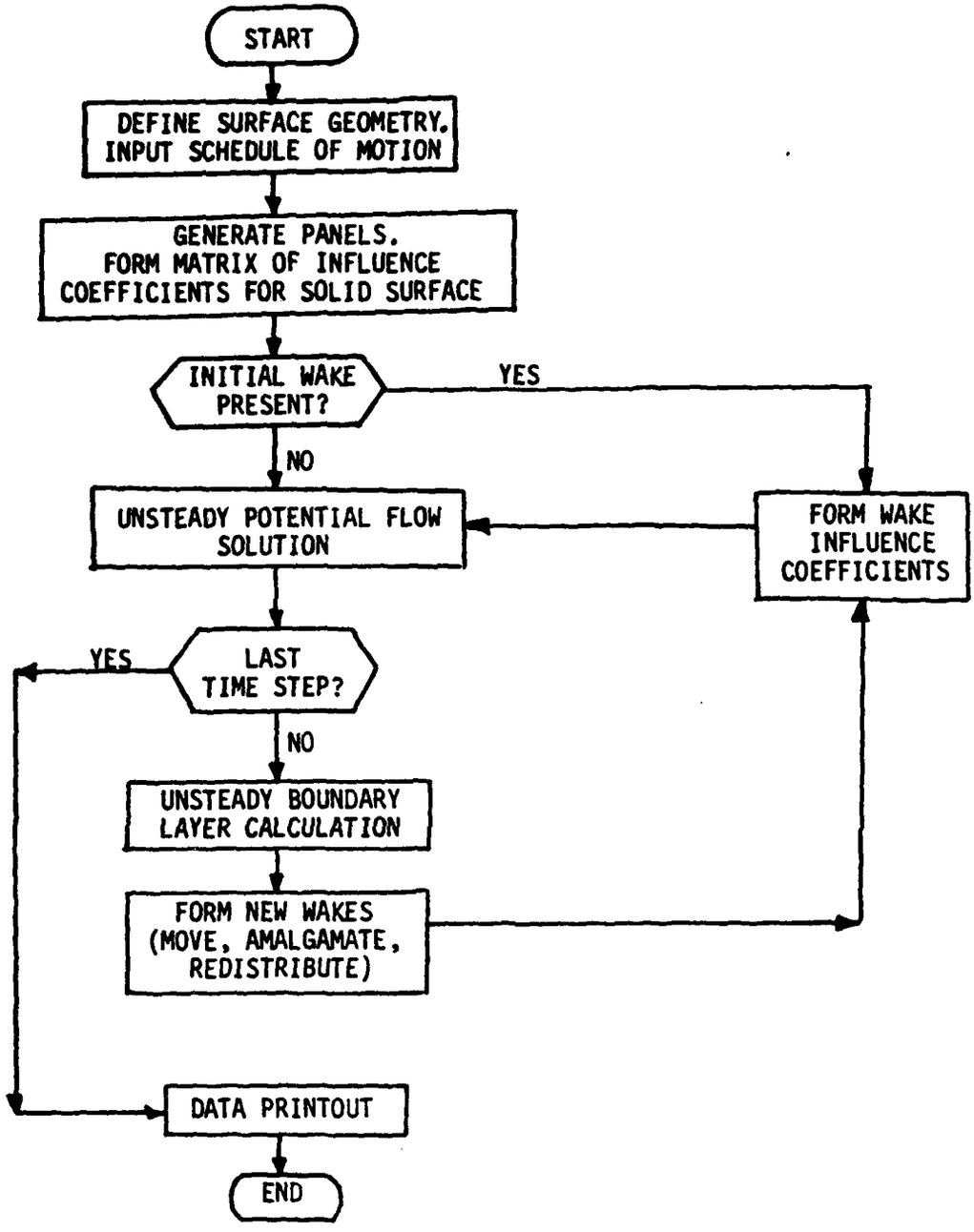

Figure 16. Flow Diagram for the Combined Code.

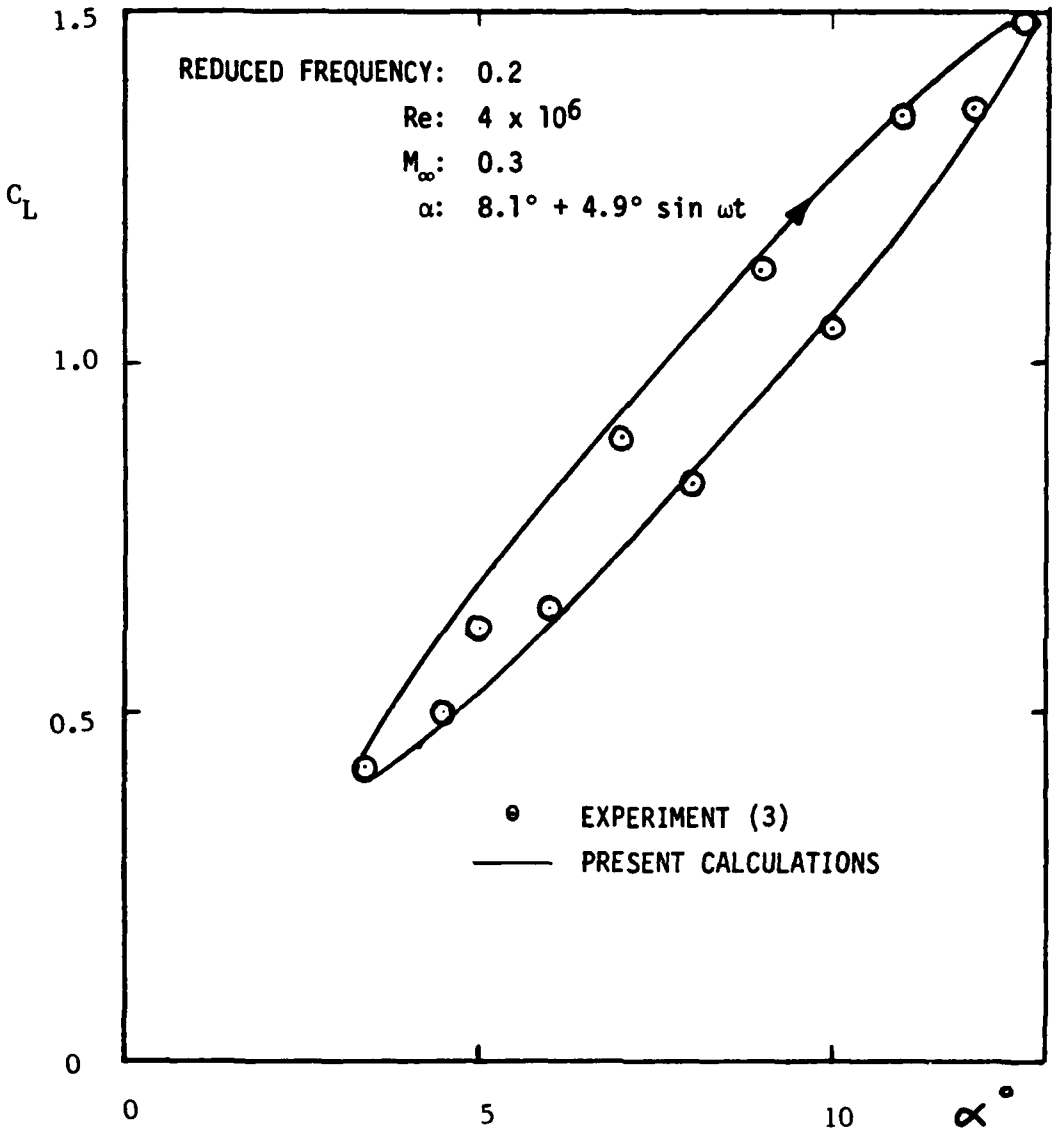

Figure 17. Comparison of Calculated and Measured Lift on a NACA 0012 Airfoil Oscillating in Pitch about the Quarter Chord.

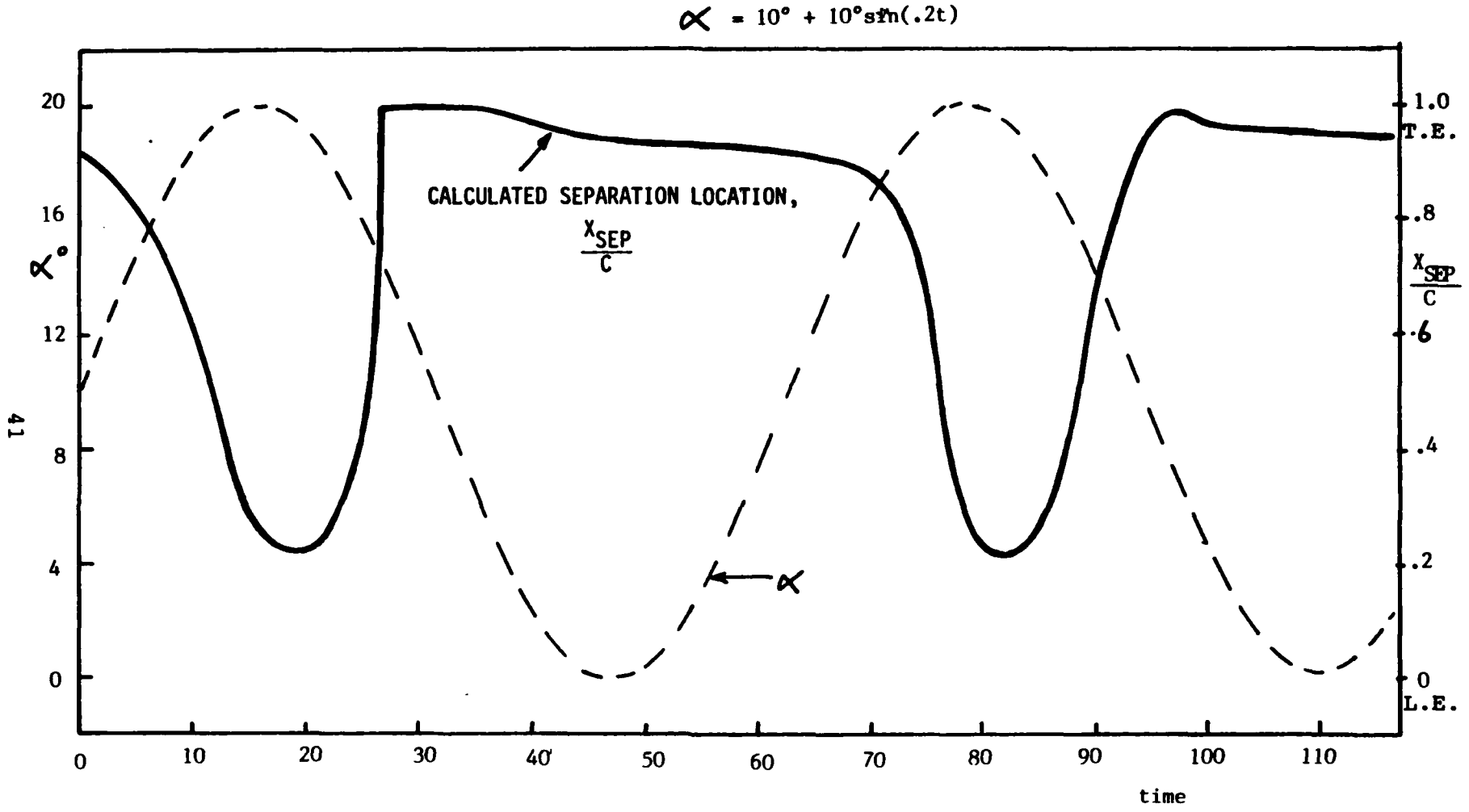

Figure 18. Calculated History of Separation Location on a NACA 0012 Airfoil Oscillating about the Quarter-Chord.

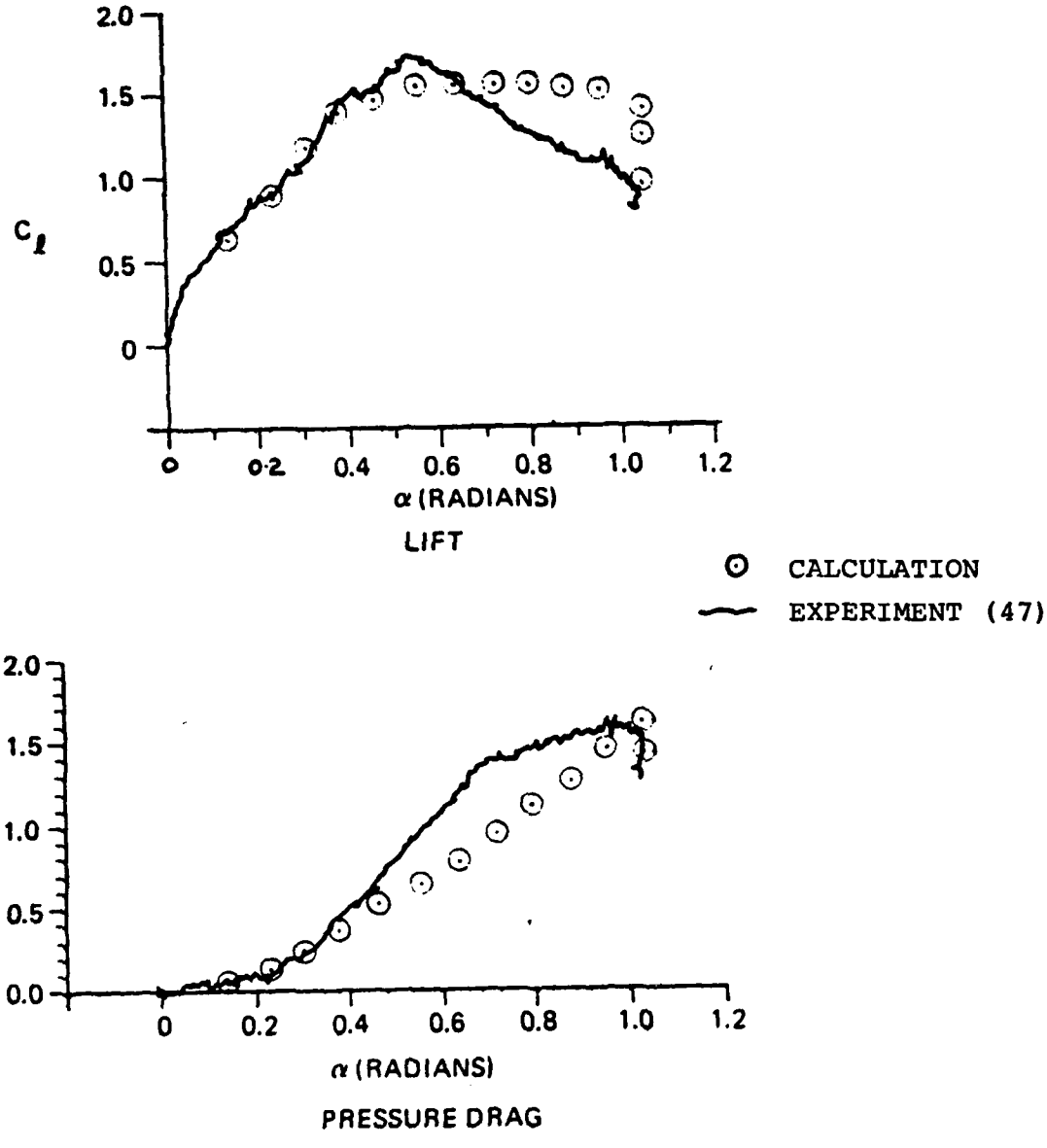

(a) k = 0.047, α_{MAX} = 60°.

Figure 19. Comparison of Calculated and Measured Lift and Pressure Drag on a NACA 0012 Section During Pitch-up Motion about x/c = .317.

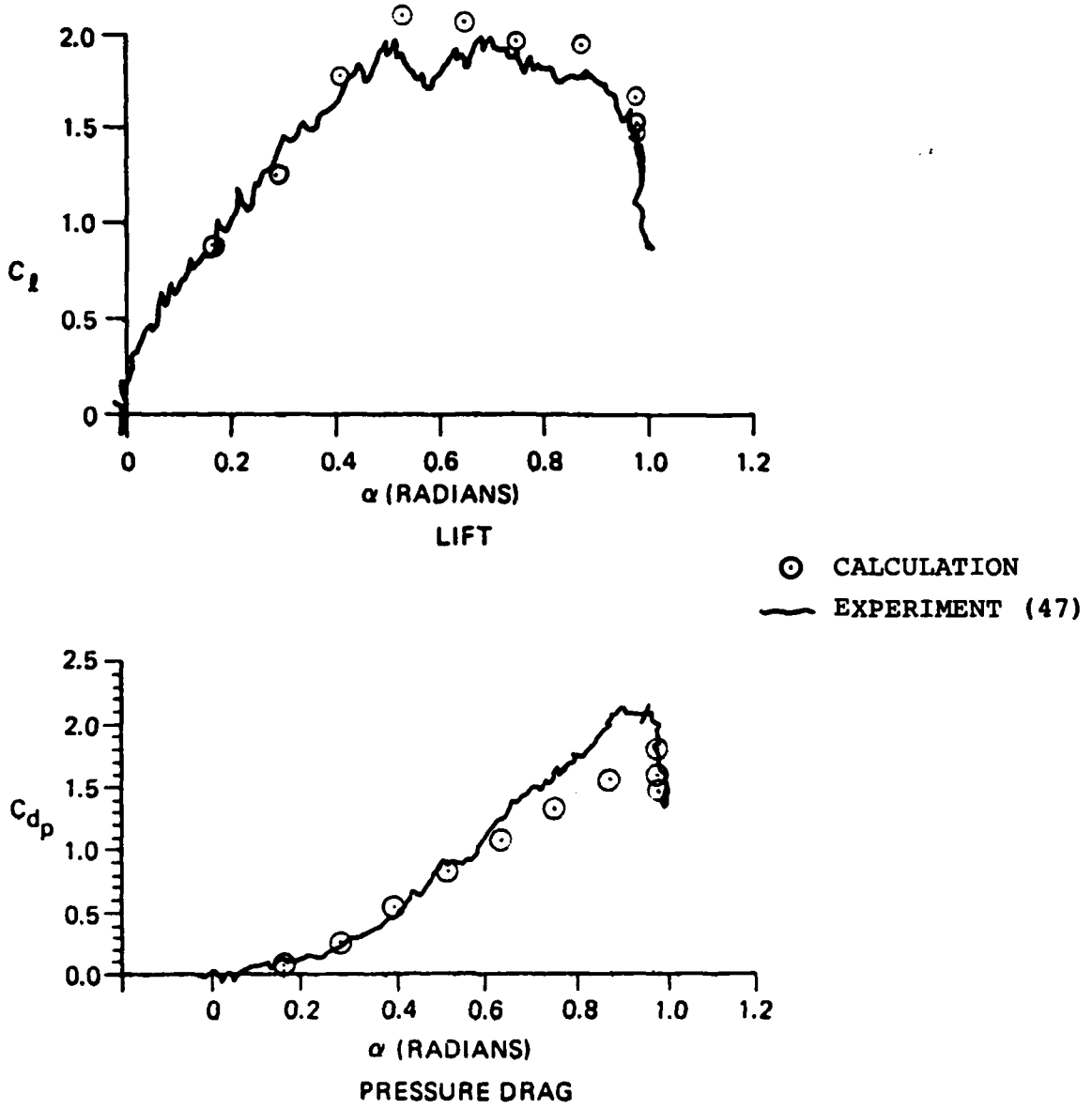

(b) k = 0.089, α_{MAX} = 56°.

Figure 19. Continued.

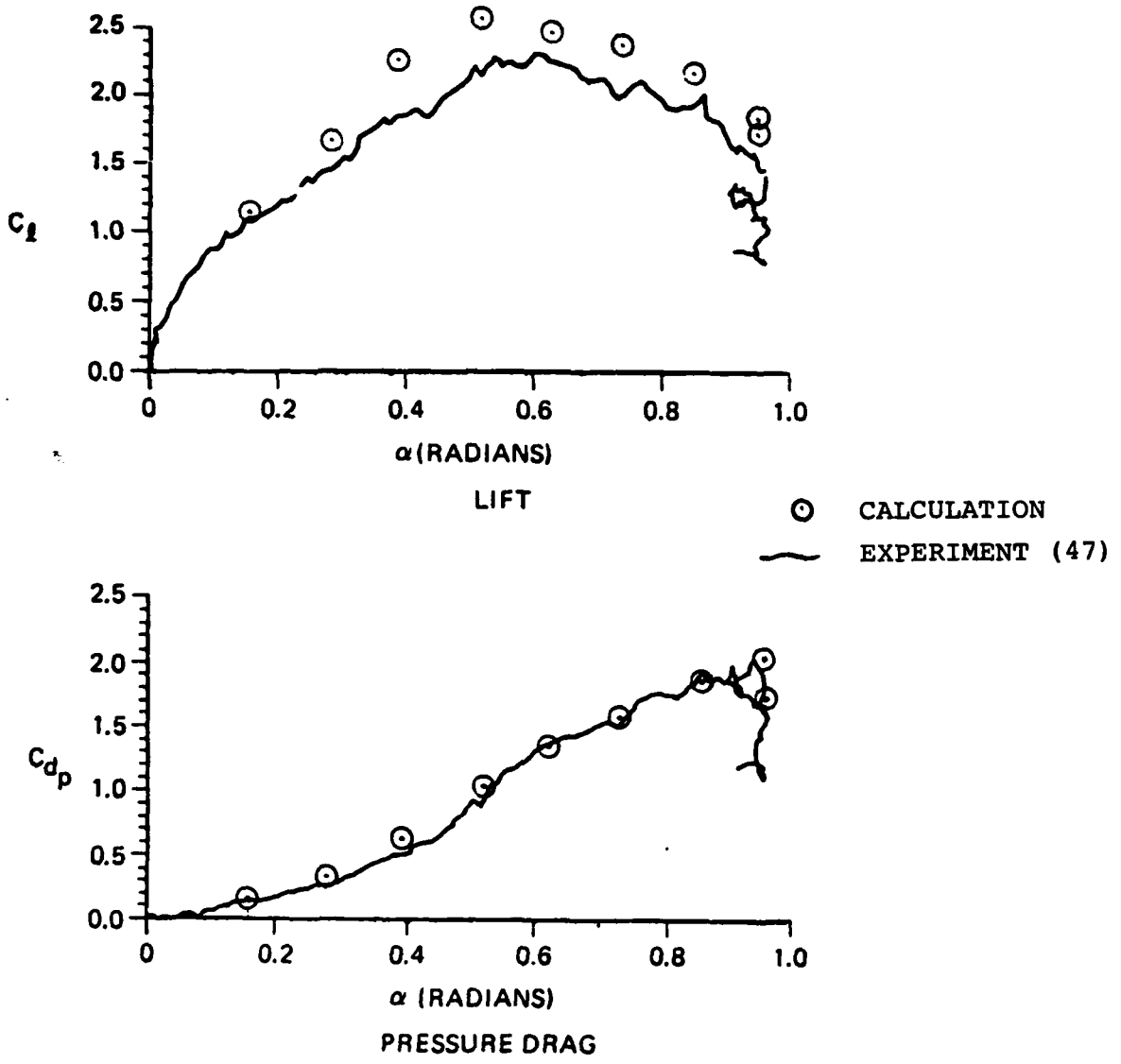

(c) k = 0.13, α_{MAX} = 55°.

Figure 19. Concluded.

this time and so further refinements are planned. In the present calculation the vortex core on the upper sheet did not "condense" early enough in the amalgamation procedure; consequently, the vortex formed just downstream of the trailing edge and did not closely interact with the airfoil surface during the pitch-up phase. This tendency was still present at the higher pitch-up rates, k = .089 and k = .13, but to a lesser extent. In these cases the calculated lift and drag characteristics, Figures 19(b) and (c), respectively, are in very good agreement with experiment. The tendency for the measured lift to peak at about α = 30° is also shown in the calculated results. These calculations were not continued at α_{max} for a sufficient time to enable "steady-state" conditions to be reached. As stated earlier, because of problems with the amalgamation routine, a strong vortex core did not "condense" for these cases and so the upper surface suction peak seen in the experimental measurements (47) did not materialize; rather, a smeared suction peak appeared because of the more diffuse region of shed vorticity. Consequently, although the integrated lift and drag are in good agreement, the pitching moment characteristic (not shown) is not satisfactory at this time. This upper surface suction peak, which is associated with a reversed flow region under the vortex, was, in fact, computed in earlier preliminary calculations (see Figure 13) involving a higher pitch rate, k = .175. In this case a vortex core condensed early in the calculation (Figure 13(a)).

Overall these calculations are very encouraging and with some refinement in the vortex amalgamation procedure, it is anticipated that the details of the unsteady pressure distributions will be achieved.

Although the two-dimensional pilot program was generated primarily as a tool to examine the behavior of various parts of the dynamic separation calculation, it has shown considerable promise as a general purpose code for two-dimensional calculations. Earlier examples (e.g., Figures 10, 11 and 12) demonstrated a capability to compute base pressures and drag coefficients of blunt sections using an impulsive start. An extension of this to compute spoiler characteristics has also been briefly examined. Figure 20 shows computed wake configurations at two steps. This is for the case of a spoiler deflected 30° on an airfoil at α = 8°. The final base pressure and integrated lift, Figure 20 (b) and (c), respectively, are in good agreement with experimental measurements (48). The calculated values represent an average value over the last few time steps as the solution had started to oscillate. The amplitude on C_L is about .1 but the calculation ought to be continued for a longer time to examine whether a pattern between upper and lower vortex formation is established. This application could be extended further to examine pitch rates and, with a straightforward extension of the code, rates of spoiler deployment. Such an extension, involving relative motion between parts of the configuration, would also allow treatment of pitching airfoils between channel walls to

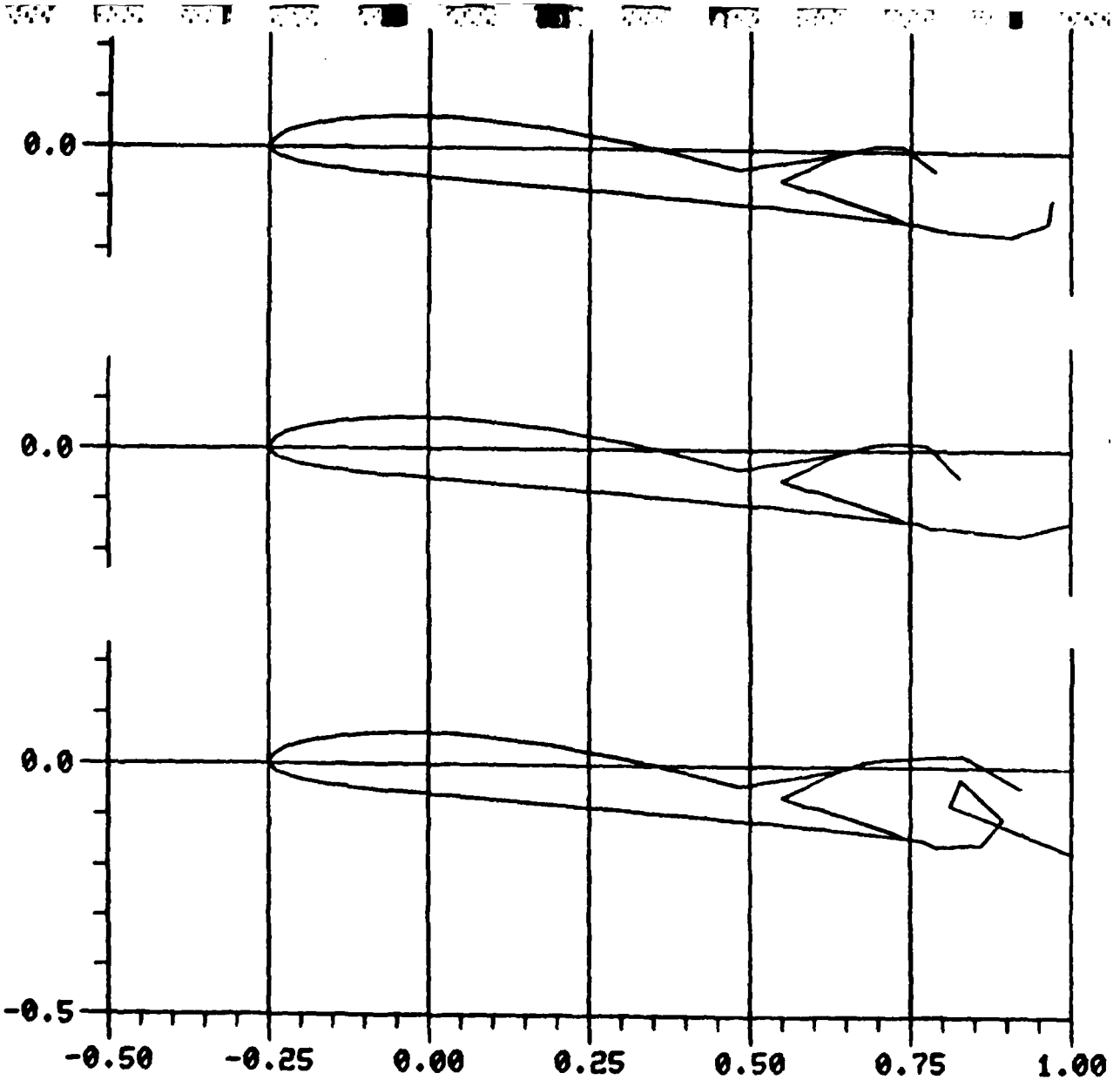

(a) Samples from Computed Wake Development.

Figure 20. Airfoil with Spoiler Deflected 30°.

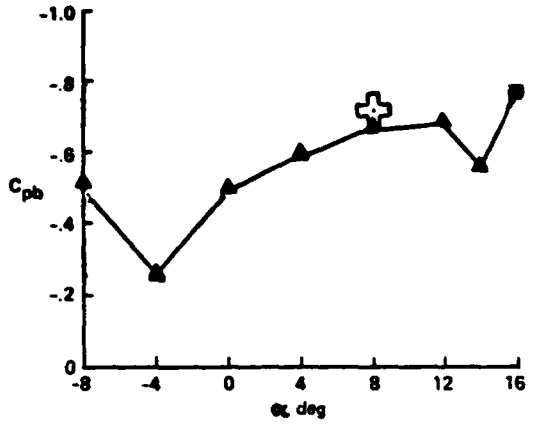

(b) Base Pressure Behind Spoiler.

▲ EXPERIMENT (48)

✚ PRESENT CALCULATION

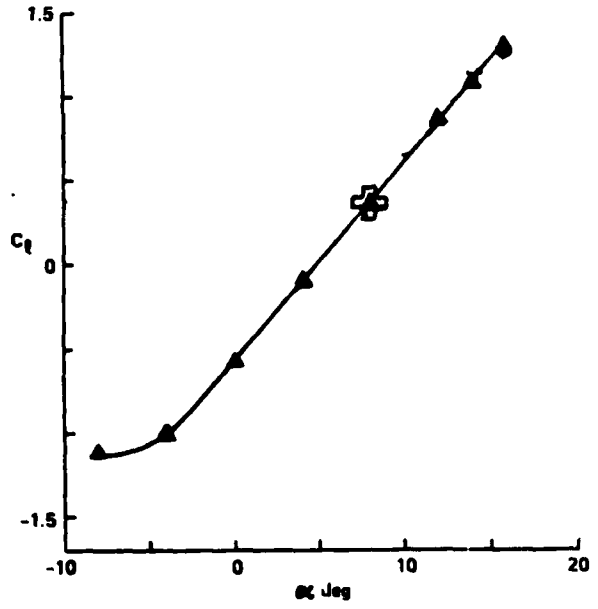

(c) Lift Coefficient.

Figure 20. Concluded.

assess the effects of unsteady blockage in pitch-up or oscillatory experiments.

While the two-dimensional program has been used to examine and develop the various routines required for the coupled dynamic separation calculations, the three-dimensional code development has been following closely behind. The unsteady boundary layer calculation--which is performed along computed surface (external) streamlines at each time step--has been fully coupled with the unsteady inviscid program. Test cases have been performed and compared with experimental data from the DFVLR-AVA in Göttingen. These experiments were conducted as part of a cooperative agreement between the DFVLR Institute of Aeroelasticity/West Germany and NASA Langley Research Center. Figure 21 compares the calculated and measured real and imaginary pressure distributions at a 70% spanwise station on an AR = 4 rectangular wing undergoing pitch oscillation about the quarter chord with $\alpha = 7.9^{o} + 1.0^{o}$ sin (.2t). (Reynolds number is 1.35×10^{6}.) The potential flow solution is also shown to indicate the extent of the viscous correction. The complete solution is in very good agreement with the measurements. This is still true for the condition, $\alpha = 12^{o} + 1.0^{o}$ sin (.3t), which is approaching the condition of dynamic stall onset; a pressure deviation is apparent near the leading edge. Work is continuing on further development of the three-dimensional method, incorporating the techniques that are being examined in the two-dimensional pilot code.

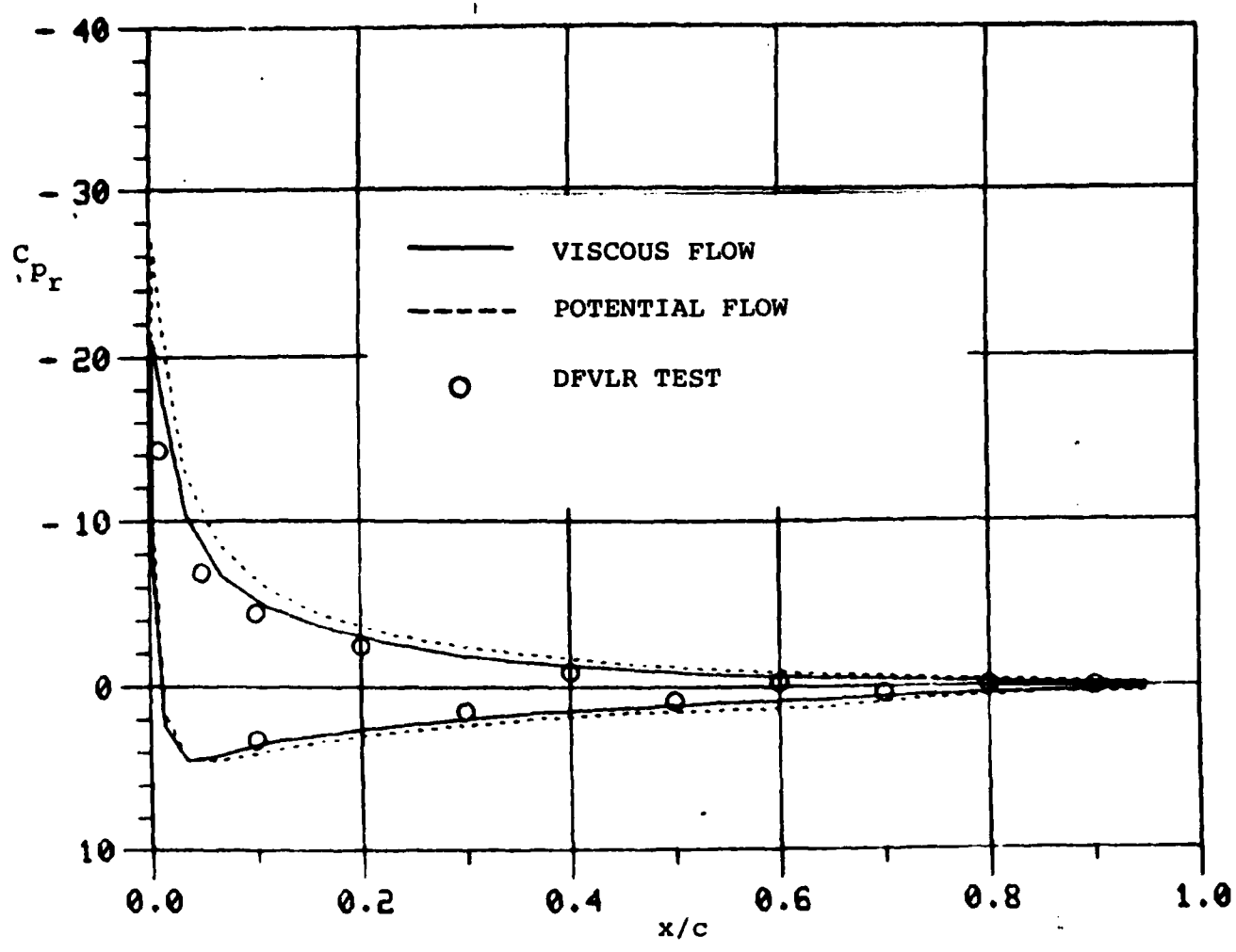

Figure 21(a) (i). Comparison of Chordwise Pressure Distribution (Real Part) at y/s = 0.70 between Computed and DFVLR Data (α_o = 7.9°, α_i = 1°, k = 0.2).

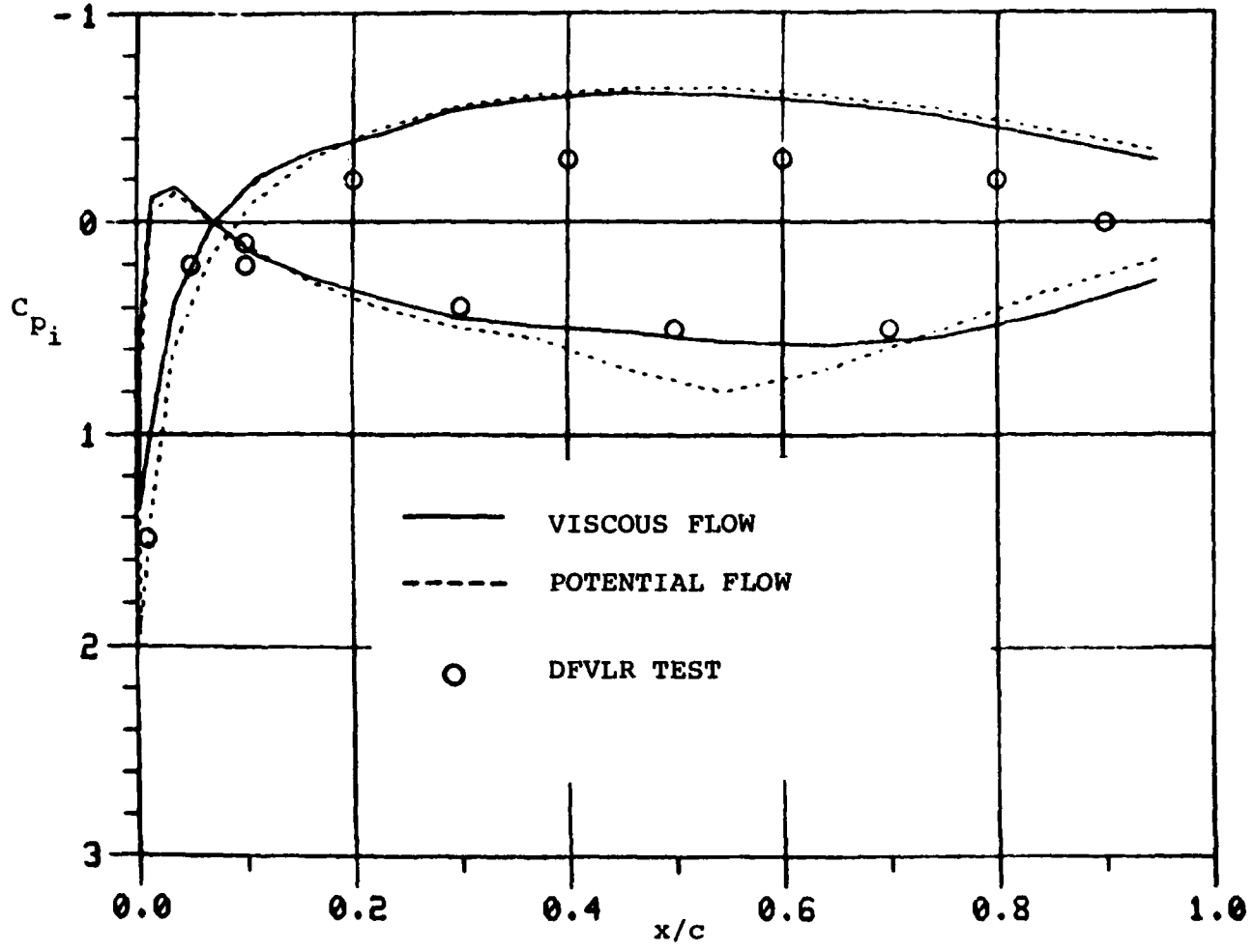

Figure 21(a) (ii). Comparison of Chordwise Pressure Distribution (Imaginary Part) at y/s = 0.70 between Computed and DFVLR Data (α_o = 7.9°, α_i = 1°, k = 0.2).

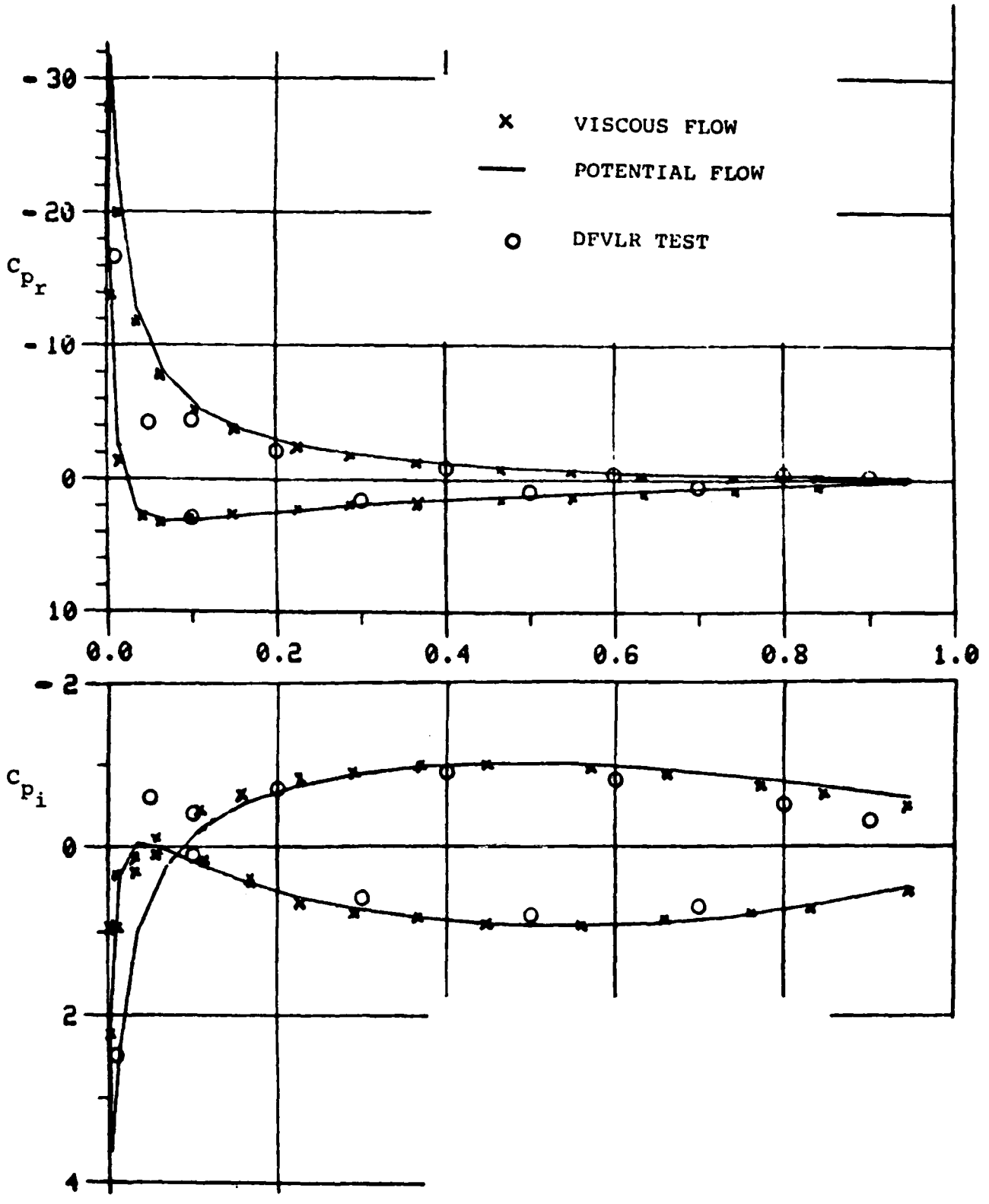

Figure 21(b). Comparison of Chordwise Pressure Distribution between Computed and DFVLR Data (α_o = 12°, α_i = 1.07; k = .3, Rn = 1.35 x 10^6; Spanwise Location, η = 0.7.

5.0 CONCLUSIONS

A system of routines has been developed to couple an unsteady time-stepping potential flow panel method with an extensive separation model and an unsteady boundary layer code. The routines include treatment of the growth of a multiple sheet dynamic wake model and also the movement of the separation location with time. Preliminary checkout of the routines using a simplified pilot code show encouraging results for conditions approaching the onset of dynamic stall. These test calculations have shown that the current boundary layer procedure is capable of predicting the unsteady boundary layer development and it should be adequate for analyzing dynamic stall.

Calculations for constant-rate pitch-up to about 60° angle of attack have shown encouraging agreement with experimental measurements but have uncovered a weakness in the vortex amalgamation routine in the pilot program Further refinements are therefore planned for the vortex wake treatment. Work is continuing to install the pilot program routines in the three-dimensional program in order to continue the investigation of the coupled viscous/inviscid approach to dynamic separated flow calculation.

6.0 REFERENCES

1. McCroskey, W.J., "Recent Developments in Dynamic Stall", Proc. Symposium on Unsteady Aerodynamics, Univ. of Arizona, Tuscon, AZ, Vol. I, March 1975, pp. 1-33.

2. McCroskey, W.J., "Prediction of Unsteady Separated Flows on Oscillating Airfoils", AGARD Lecture Series on Three-Dimensional and Unsteady Separated Flow at High Reynolds Numbers, VKl, Belgium, AGARD LS-94, Paper 12, February 1978.

3. McCroskey, W.J., McAlister, K.W., Carr, L.W., Pucci, S.L., Lambert, O and Indergand, Lt. R.F., "Dynamic Stall on Advanced Airfoil Sections", Paper 80-01 in Proc. 36th Annual Forum AHS, May 1980.

4. Maskew, B., "Influence of Rotor Blade Tip Shape on Tip Vortex Shedding--An Unsteady Inviscid Analysis", Paper 80-6 in Proc. 36th Annual Forum of AHS, May 1980.

5. Maskew, B., Rao, B.M. and Dvorak, F.A., "Prediction of Aerodynamic Characteristics for Wings with Extensive Separations", Paper No. 31 in AGARD-CPP-291, September 1980.

6. Maskew, B., "Prediction of Subsonic Aerodynamic Characteristics--A Case for Low-Order Panel Methods", Paper 81-0252, Presented at AIAA 19th Aerospace Sciences Meeting, St. Louis, MO, January 1981.

7. Liiva, J. et al., "Two-Dimensional Tests of Airfoils Oscillating near Stall", U.S. Army Aviation Material Lab., Ft. Eustis, VA, Technical REport 68-13, April 1968; also J. Aircraft, Vol. 6y, No. 1, January 1979, pp. 46-51.

8. Lang, J.D., "Experimental Results for an Airfoil with Oscillating Spoiler and Flap", Symposium on Unsteady Aerodynamics, Kinney, R.B., ed., Univ. of Arizona, Tuscon, AZ, 1975, pp. 55-80; also j. Aircraft, Vol. 13, No. 9, September 1976, pp. 687-694.

9. Lang, J.D. and Francis, M.S., "Dynamic Loading on an Airfoil due to a Growing Separated Flow", Paper 26 in "Prediction of Aerodynamic Loading", AGARD CP-204, 1976.

10. Maresca, C., Rebont, J. and Valensi, J., "Separation and Reattachment of the Boundary Layer on a Symmetrical Airfoil Oscillating at Fixed Incidence in a Steady Flow", Symposium on Unsteady Aerodynamics, Kinney, R.B., ed.; Univ. of Arizona, Tuscon, AZ, 1975, pp. 35-53.

11. Saxena, L.S., Fejer, A.A. and Jorkovin, M.V., "Effects of Periodic Changes in Free Stream Velocity on Flows over Airfoils near Static Stall", Nonsteady Fluid Dynamics, eds., Crow, D.E. and Miller, J.A.; December 1978, pp. 111-116.

12. Ericson, L.E. and Reding, J.P., "Dynamic Stall at High Frequency and Large Amplitude", J. Aircraft, Vol. 17, No. 3, March 1980, pp. 136-142.

13. Carr, L.W., McAlister, K.W. and McCroskey, W.J., "Analysis of the development of Dynamic Stall Based on Oscillating Airfoil Experiments", NASA TN D-8382, January 1977.

14. Ham, N.D., "Aerodynamic Loading on a Two-Dimensional Airfoil during Dynamic Stall", AIAA J., Vol. 6, No. 10, October 1968, pp. 1927-1934.

15. Baudu, N., Sanger, M. and Souquet, J., "Modelisation du Decrochage Dynamique d'un Profil Oscillant", AAAF 10th Colloque d'Aerodynamique Appliquee", Lille, France, November 1973.

16. McCroskey, W.J. and Philippe, J.J., "Unsteady Viscous Flow on Oscillating Airfoils", AIAA J., Vol. 13, No. 1, January 1975, pp. 71-79.

17. Scrugges, R.M., Nash, J.F. and Singleton, R.E., "Analysis of Dynamic Stall using Unsteady Boundary Layer Theory", NASA CR-2467, October 1974.

18. McCroskey, W.J., "Introduction to Unsteady Aspects of Separation in Subsonic and Transonic Flow", Paper 6, AGARD LS-94, February 1978.

19. Sears, W.R. and Teleoniz, D.P., "Boudary Layer Separation in Unsteady Flow", SIAM J. Appl. Math., Vol. 28, No. 1, January 1975, pp. 215-235.

20. Crimi, P. and Reeves, B.L., "A Method for Analyzing Dynamic Stall of Helicopter Rotor Blades", NASA CR-2009, May 1972.

21. Shamroth, S.J. and Kreskovsky, J.P., "A Weak Interaction Study of the Viscous Flow about Oscillating Airfoils", NASA CR-132425, May 1974.

22. MacCormack, R.W., "Status and Future Prospects of Using Numerical Methods to Study Complex Flows at High Reynolds Numbers", Paper 13, AGARD LS-94, February 1978.

23. Roberts, A. and Rundle, K., "Computation of Incompressible Flow about Bodies and Thick Wings using the Spline Mode System", BAC (CAD) Report MA 19, 1972.

24. Hess, J.L. and Martin, R.P., Jr., "Improved Solution for Potential Flow about Arbitrary axisymmetric Bodies by the Use of a Higher-Order Surface Source Method", NASA CR-134694, July 1974.

25. Johnson, F.T. and Rubbert, P.E., "A General Panel Method for the Analysis and Design of Arbitrary Configurations in Subsonic Flows", NASA CR-3079, 1980.

26. Bristow, D.R. and Grose, G.G., "Modification of the Douglas Neumann Program to Improve the Efficiency of Predicting Component Interference and High Lift Characteristics", NASA CR-3020, 1978.

27. Maskew, B., "Calculation of Two-Dimensional Vortex/Surface Interference using Panel Methods", NASA CR-159334, December 1980.

28. Morino, L., Chen, L.-T. and Suci, E.O., "Steady and Oscillatory Subsonic and Supersonic Aerodynamics around Complex Configurations", AIAA J., Vol. 13, No. 3, March 1975.

29. Seetharam, H.C., "Experimental Investigation of Separated Flow Fields on an Airfoil at Subsonic Speeds", Ph.D. Dissertation, Wichita State University, March 1975.

30. Maskew, B. and Dvorak, F.A., "The Prediction of CLMAX using a Separated Flow Model", J. Am. Hel. Soc., April 1978.

31. Dvorak, F.A., Maskew, B. and Rao, B.M., "An Investigation of Separation Models for the Prediction of CLMAX", Final Technical Report Prepared for the U.S. Army Research Office, Research Triangle Park, N.C., 1976-1979.

32. Young, W.J., Jr. and Hoad, D.R., "Comparison of Flow Surveys above Stalled Wings", AIAA Paper 79-0174, January 1979.

33. Gross, L.W., "The Prediction of Two-Dimensional Airfoil Stall Progression", AIAA Paper NO. 78-155, January 1978.

34. Zumwalt, G.W. and Naik, S.N., "An Analytical Method for Highly Separated Flow on Airfoils at Low Speeds", Wichita State University Aeronautical Report 77-2, May 1977.

35. Henderson, M.L., "A Solution to the Two-Dimensional Separated Wake Modeling Problem and its Use to Predict CLMAX of Arbitrary Airfoil Sections", AIAA Paper 78-156, January 1978.

36. Jacob, K., "Advancement of a Method for Calculating Separated Flows around Airfoils with Special Consideration of Profile Drag", DLR-FB-76-36, Translated at ESA-TT-373, April 1977.

37. Rao, B.M., Maskew, B. and Dvorak, F.A., "Prediction of Aerodynamic Characteristics of Fighter Wings at High Lift", ONR Report CR-215-258-1, July 1979.

38. Dvorak, F.A. and Maskew, B., "The Modelling of Airfoil Separation in Subsonic and Transonic Flow", Paper No. 1 in Proc. 5th U.S. Air Force and Federal Republic of Germany Data Exchange Agreement Meeting, AFWAL-TR-80-3088, June 1980, pp. 1-22.

39. Moore, D.W., "A Numerical Study of Roll-up of a Finite Vortex Sheet", J. Fluid Mech., Vol. 63, No. 2, 1974, pp. 225-235.

40. Fink, P.T. and Soh, W.K., "A New Approach to Roll-up Calculations of Vortex Sheets", Proc. Royal Society of London, Series A, Vol. 362, 1978, pp. 195-209.

41. Sarpkaya, T. and Schoaff, R.L., "Inviscid Model of Two-Dimensional Vortex Shedding by a Circular Cylinder", AIAA J., Vol. 17, No. 11, November 1979, pp. 1193-1200.

42. Curle, N., "A Two-Parameter Method for Calculating the Two-Dimensional Incompressible Laminar Boundary Layer", J. R. Aero. Soc., Vol. 71, 1967.,

43. Cousteix, J. and Houdeville, R., "Singularities in Three-Dimensional Turbulent Boundary Layer Calculation and Separation Phenomena", AIAA J., Vol. 19, No. 8, August 1981.

44. Lyrio, A.A. and Ferziger, J.H., "A Method of Predicting Unsteady Turbulent Flows and its Application to Diffusers with Unsteady Inlet Conditions", AIAA J., Vol. 21, No. 4, April 1983.

45. Cousteix, J., Private Communication.

46. Nash, J.F., Carr, L.W. and Singleton, R.E., "Unsteady Turbulent Boundary Layers in Two-Dimensional, Incompressible Flow", AIAA J., Vol. 13, No. 2., February 1975.

47. Francis, M.S., Keesee, J.E. and Retelle, J.P., Jr., "An Investigation of Airfoil Dynamic Stall with Large Amplitude Motions", Frank J. Seiler Research Laboratory Report FJSRL-TR-80-0010, October 1983.

48. McLachlan, B.G. and Karamcheti, K., "Experimental Study of the Flow Field of an Airfoil with Deflected Spoiler", Paper 82-0126, Presented at AIAA 20th Aerospace Sciences Meeting, Orlando, Florida, January 1982.

END

FILMED

1-85

DTIC